Mrk421 and Mrk501 as high-energy physics laboratories to study the nature of blazars

David Paneque (MPP/ICRR)
(dpaneque@mppmu.mpg.de)
M. Doert, L. Fortson, S. Jorstad, A. Marscher,
N. Nowak, R. Lico, A. Pichel, S. Sun, H. Takami,
on behalf of the *Fermi*-LAT, MAGIC, VERITAS collaborations
GASP-WEBT, F-GAMMA, and many participants

Outline

- Introduction
- Extensive MW campaigns on Mrk421 and Mrk501
- Highlight results from the first campaigns (from 2009 to 2011)

  → See poster 8.11, from Amy Furniss, for results from the campaigns from 2013, which includes NuSTAR and the upgraded MAGIC/VERITAS
- Conclusions

1 - Introduction

See talks from M. Hayashida & A .Reimer

It is VERY CHALLENGING to study blazars

From Observational perspective, there are two major practical challenges

a) Blazars emit over a very wide energy range (from radio to very high energy gamma-rays)

Emission in different energy bands could be produced by same population of particles

→ *Need many instruments (covering many bands) to fully study these objects*

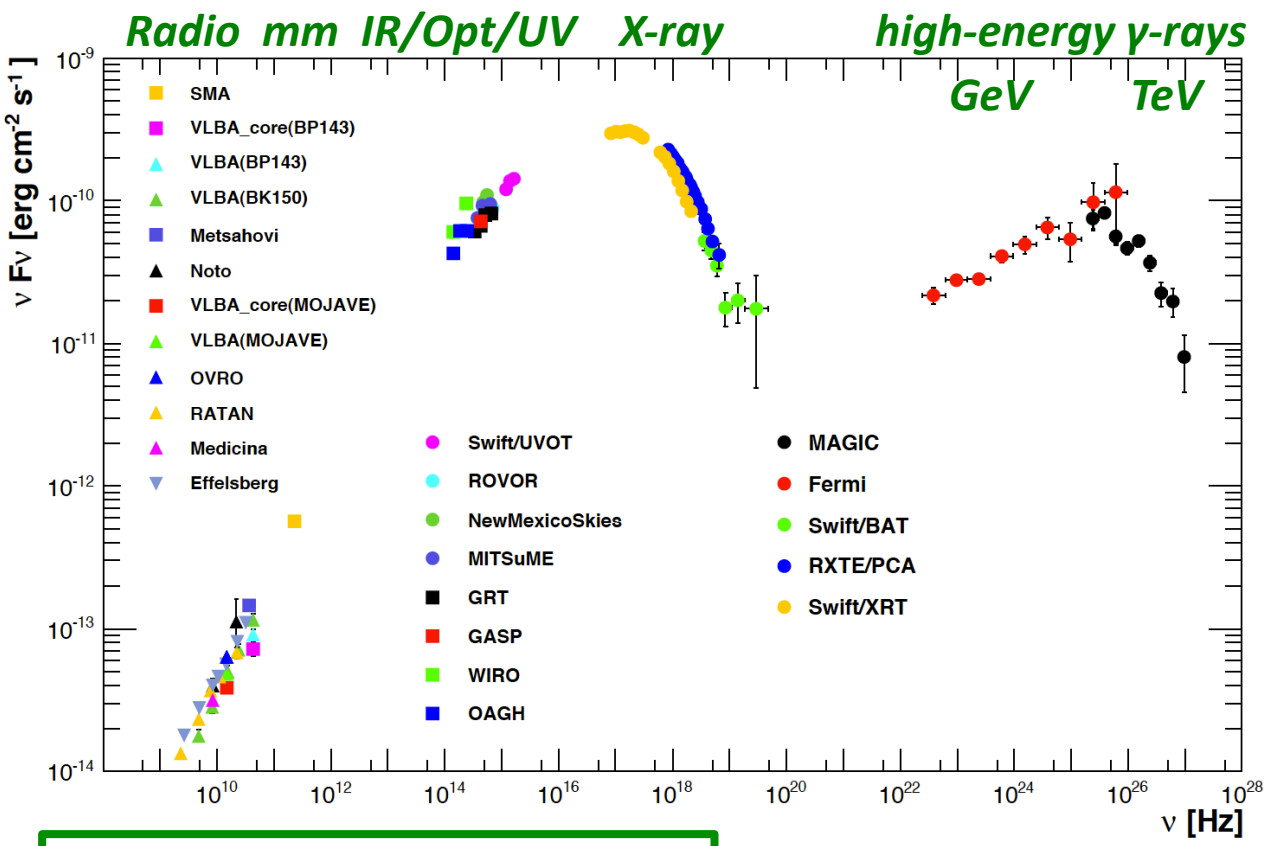

Spectral energy distribution (SED) of the Blazar Markarian 421

Abdo et al 2011, ApJ 736, 131

1 - Introduction

See talks from M. Hayashida & A .Reimer

It is VERY CHALLENGING to study blazars

From Observational perspective, there are two major practical challenges

a) Blazars emit over a very wide energy range (from radio to very high energy gamma-rays)

Emission in different energy bands could be produced by same population of particles

→ *Need many instruments (covering many bands) to fully study these objects*

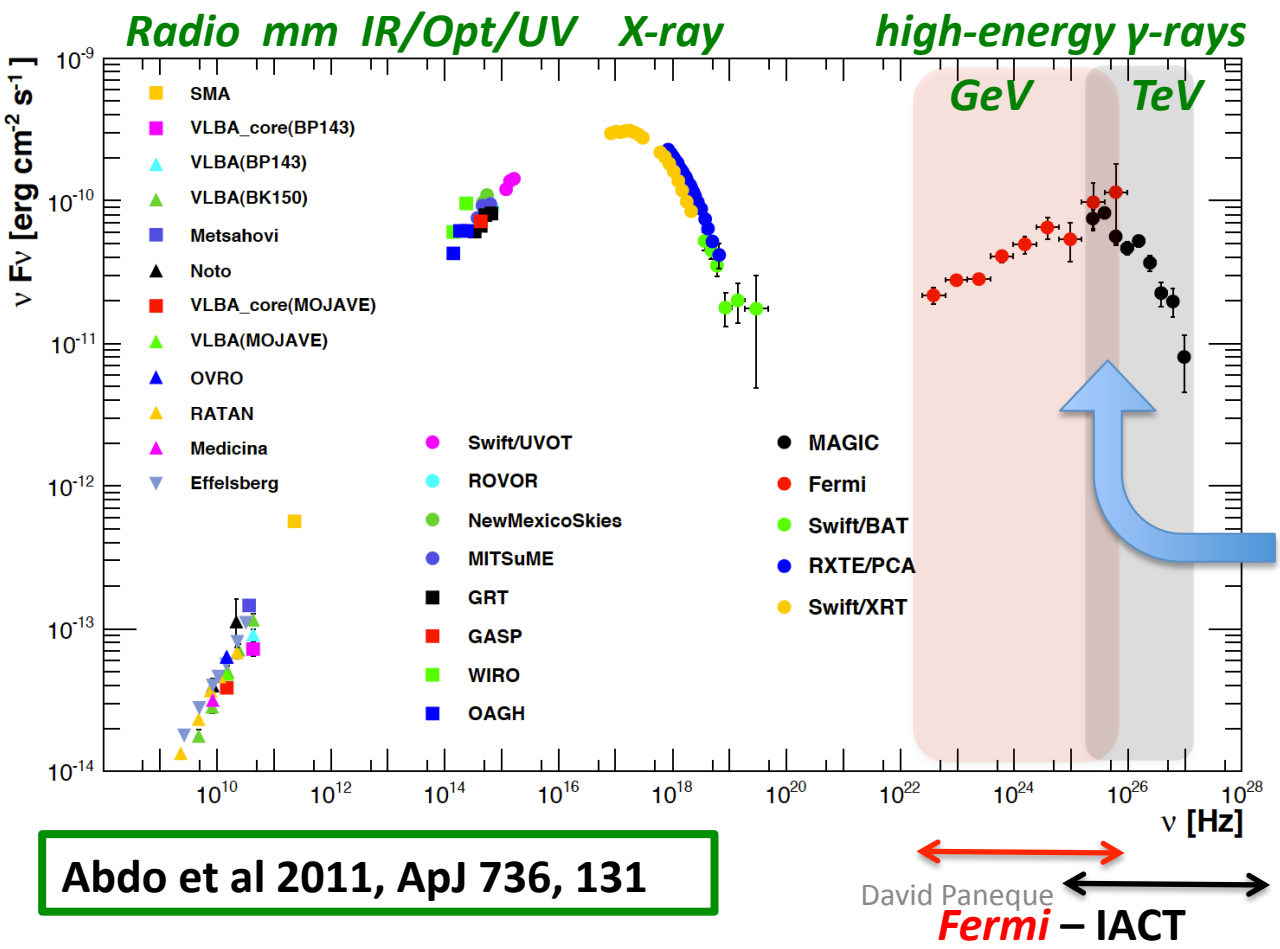

Abdo et al 2011, ApJ 736, 131

Spectral energy distribution (SED) of the Blazar Markarian 421

Gamma-ray bump could only be measured recently, with *Fermi*-LAT + modern IACTs like HESS/MAGIC/VERITAS

Fermi **– IACT** spectra cover, for the first time, the complete high energy component over 5 orders of magnitude without gaps

→ *Crucial for the theoretical modeling of the broad emission*

Fermi **– IACT**

1 - Introduction

See talks from
M. Hayashida & A .Reimer

It is VERY CHALLENGING to study blazars

From Observational perspective, there are two major practical challenges

b) Blazar emission is variable on very different timescales (from years down to minutes)

Variability connected to acceleration/radiation processes

→ *The instruments need to observe simultaneously OFTEN and during LONG BASELINES*

Mrk421 showed very distinct behavior in the 2009 and 2010 campaigns

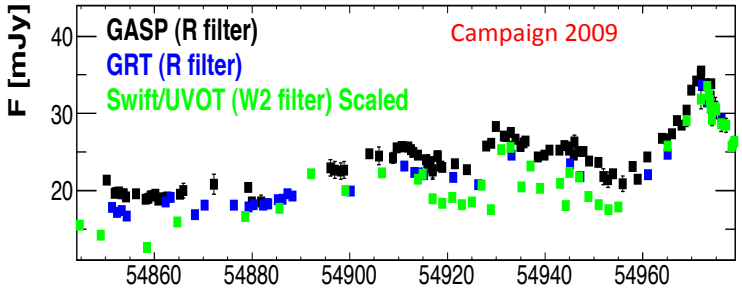

Optical

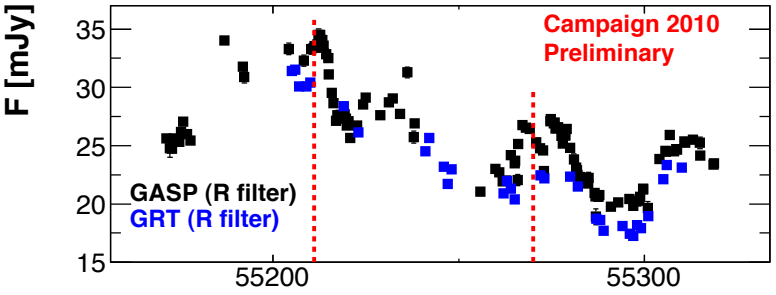

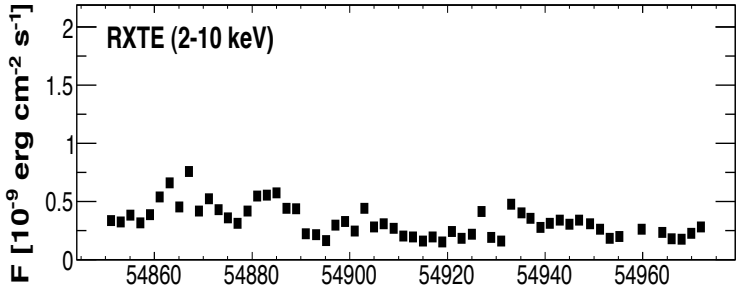

X-ray

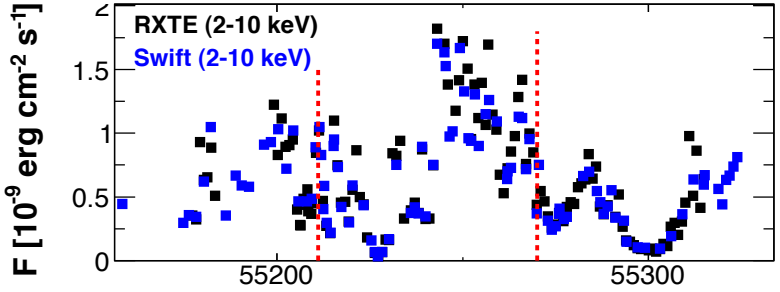

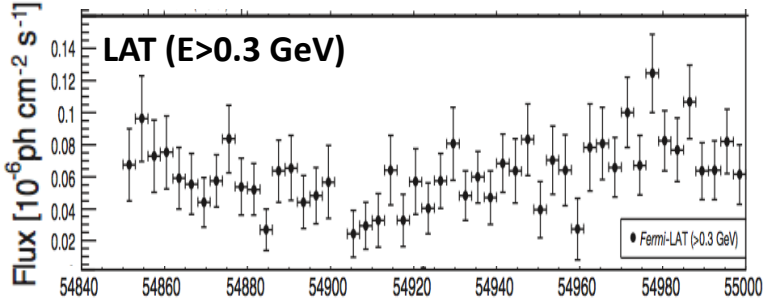

γ-ray

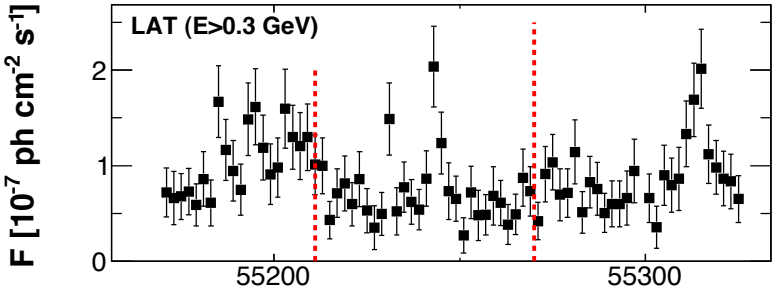

1 - Introduction

See talks from
M. Hayashida & A .Reimer

It is VERY CHALLENGING to study blazars

From Observational perspective, there are two major practical challenges

a) Blazars emit over a very wide energy range
(from radio to very high energy gamma-rays)

b) Blazar emission is variable on very different timescales
(from years down to minutes)

Studying blazars accurately requires excellent broadband (radio to gamma-rays) AND temporal (minutes to years) coverage

… like making Mochi …
Need persistency and coordination among different parties

a+b
→ Requirement for
Extensive MW campaigns
lasting for many years

2 - Extensive MW Campaigns on Mrk421 and Mrk501

Why studying Mrk421 and Mrk501 ?

- **Nearby blazars (z~0.03; ~140 Mpc)**
  - → Imaging with VLBA possible down to scales of 0.01-0.1 pc (>~ blob size)
  - → Minimal effect from EBL (among VHE blazars), which is not well known
    - → systematics for VHE blazar science

- **Bright blazars (in part also due to the fact that they are nearby)**
  - → Easy to detect with IACTs, *Fermi*, and X-rays, Optical, radio instruments in short times
    - → "Relatively Easy" to characterize the entire SED in every "shot"
      - → Can study the evolution of the entire SED

- **No strong BLR (another unknown… composition, shape…)**
  - → More simple to understand than FSRQs

In summary:

→ **Mrk421 and Mrk501 are among the "easiest" blazars to study**

It is more difficult to study other blazars that are farther away, dimmer, or have more complicated structures

Mrk421 and Mrk501 can be used as high-energy physics laboratories to study blazars

2 - Extensive MW Campaigns on Mrk421 and Mrk501

A multi-instrument and multi-year project

Since 2009, we have substantially **improved Temporal and Energy coverage** of the sources in order to obtain SEDs as simultaneous as possible, as well as to be able to perform multi-frequency variability/correlation studies over a long baseline and correlate with high resolution radio images and polarizations (to learn about the jet structure)

•More than 25 instruments participate, covering frequencies from radio to VHE

Radio: VLBA, OVRO, Effelsberg, Metsahovi…
mm: SMA, IRAM-PV
Infrared: WIRO, OAGH
Optical: GASP-WEBT, GRT, Liverpool, Kanata…
UV: Swift-UVOT
X-ray: (RXTE), Swift-XRT, NuSTAR
Gamma-ray: *Fermi*-LAT
VHE: MAGIC, VERITAS, FACT

Monitored regardless of activity (*increase coverage during flares*)
→ observed every few days for about half year (*every year* !)

3 – Highlight results from first MW campaigns

In this talk I will report mostly on results from the campaigns from 2009 to 2011

3.1 – Variability

3.2 – Correlations

3.3 – SED modeling

3.4 - Flaring activity with a EVPA rotation

3.5 – Flaring activity with ejection of a VLBA blob

3.6 - Constrains on EBL density (backup slides)

Most results extracted from the following scientific publications

- Abdo et al., 2011 (ApJ 727, 129) + Abdo et al., 2011 (ApJ 736, 131)
- Aleksic et al 2014a (accepted in A&A, **arXiv:1410.6391**)
- Lico et al., 2014 (accepted in A&A, **arXiv:1410.0884**)
- Aleksic et al 2014b (Submitted to A&A)
- Aleksic et al., 2014 (Submitted to A&A)

3 – Highlight results from first MW campaigns

In this talk I will report mostly on results from the campaigns from 2009 to 2011

3.1 – Variability

3.2 – Correlations

3.3 – SED modeling

3.4 - Flaring activity with a EVPA rotation

3.5 – Flaring activity with ejection of a VLBA blob

3.6 - Constrains on EBL density (backup slides)

Most results extracted from the following scientific publications

- Abdo et al., 2011 (ApJ 727, 129) + Abdo et al., 2011 (ApJ 736, 131)
- Aleksic et al 2014a (accepted in A&A, **arXiv:1410.6391**)
- Lico et al., 2014 (accepted in A&A, **arXiv:1410.0884**)
- Aleksic et al 2014b (Submitted to A&A)
- Aleksic et al., 2014 (Submitted to A&A)

See poster 8.11, by Amy Furniss, for results from the campaigns from 2013, which includes NuSTAR and the upgraded MAGIC/VERITAS

3.1 – Variability

Variability quantified following prescription from Vaughan et al. 2003

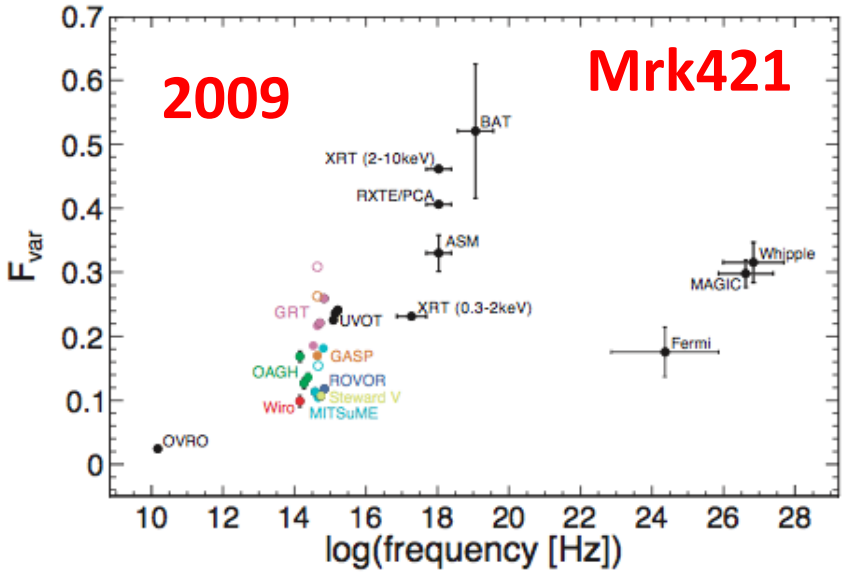

$$F_{\mathrm{var}} = \sqrt{\frac{S - \langle \sigma_{err} \rangle^2}{\langle Flux \rangle^2}}$$

Highest variability occurs at X-ray and VHE

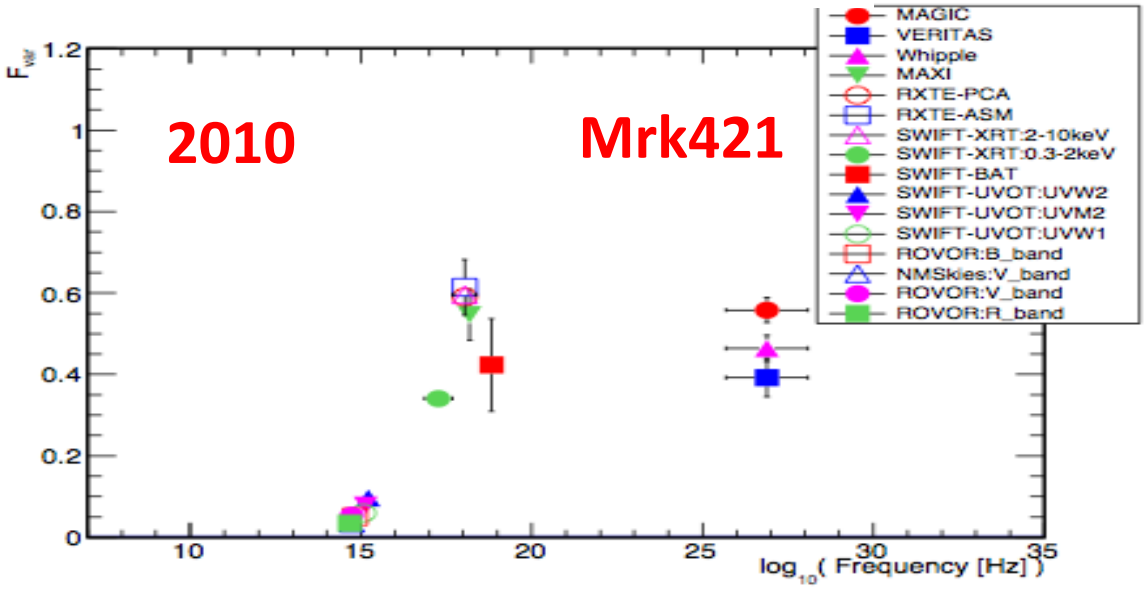

3.1 – Variability

Variability quantified following prescription from Vaughan et al. 2003

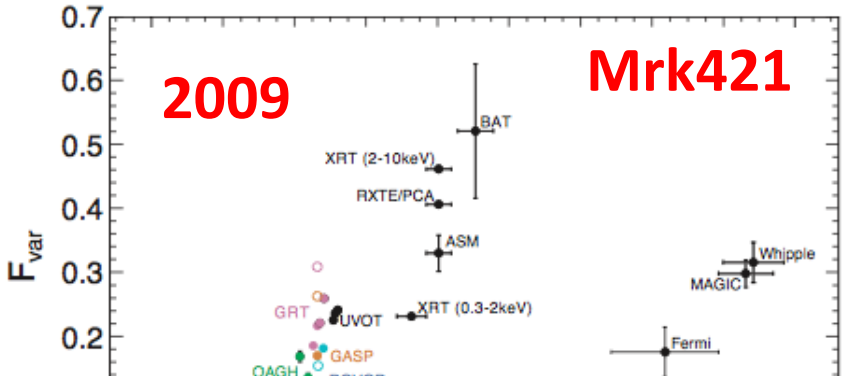

$$F_{\mathrm{var}} = \sqrt{\frac{S - \langle \sigma_{err} \rangle^2}{\langle Flux \rangle^2}}$$

Highest variability occurs at X-ray and VHE

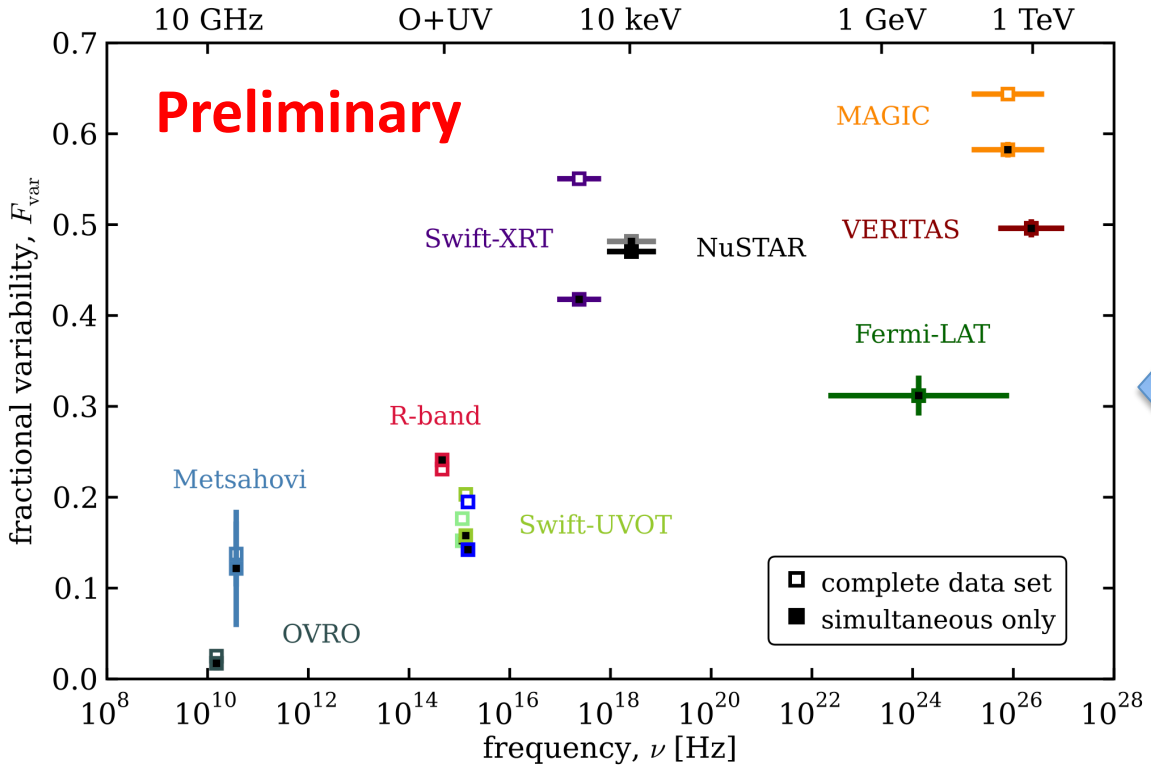

Mrk421 2013

See poster presentation from Amy Furniss (8.11)

3.1 – Variability

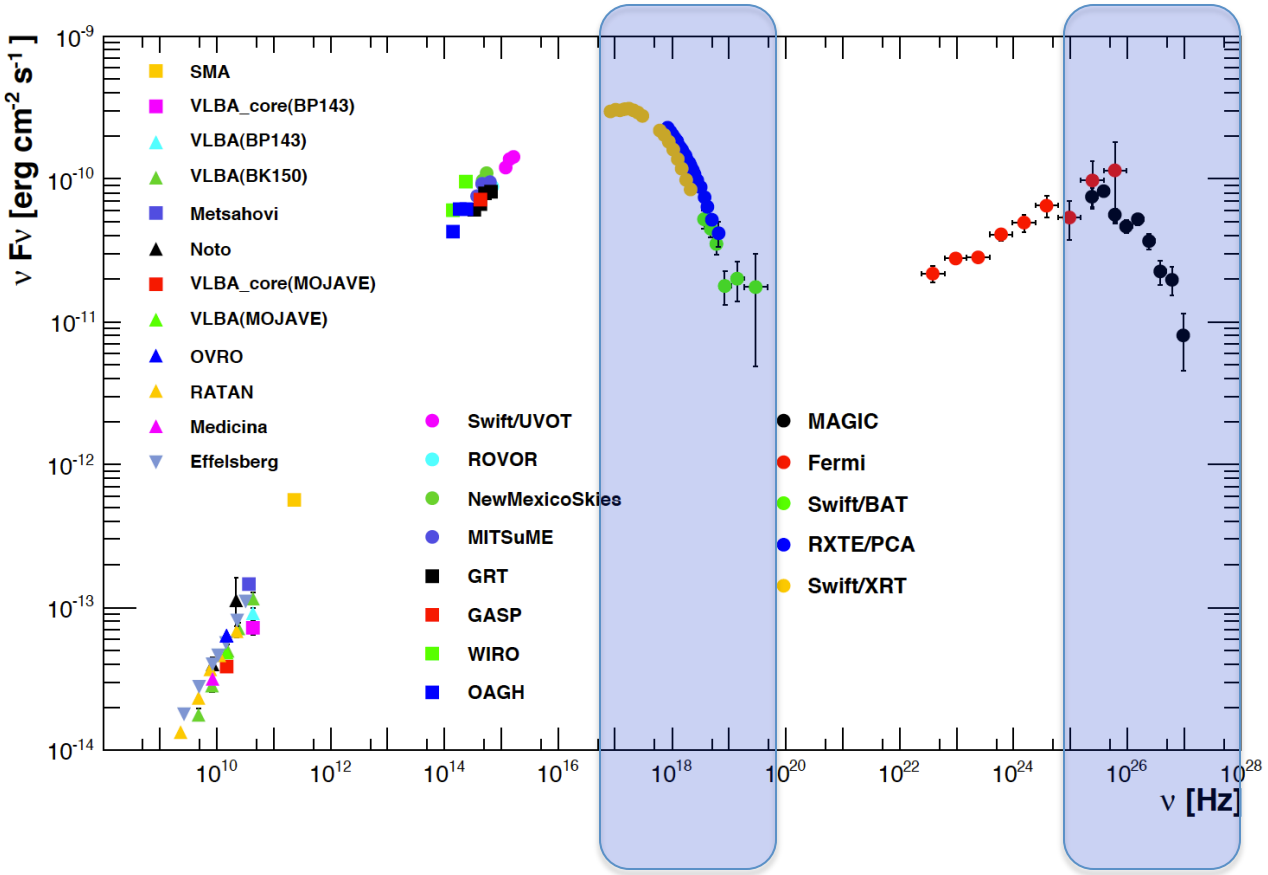

"Falling segments" of the low- and high-energy bumps are more variable than the "rising segments"

→ *Within the synchrotron self-Compton scenario, the X-ray and VHE emission is produced by the highest-energy electrons*

Fractional variability larger in the 2-10 keV than in the 0.3-2 keV

Mrk421 MW 2009

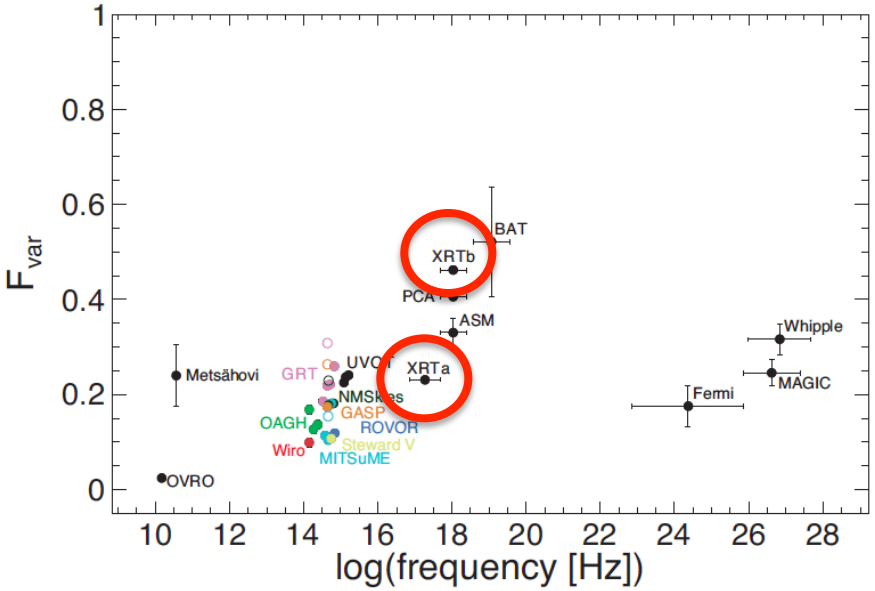

Mrk421 MW 2010 (March)

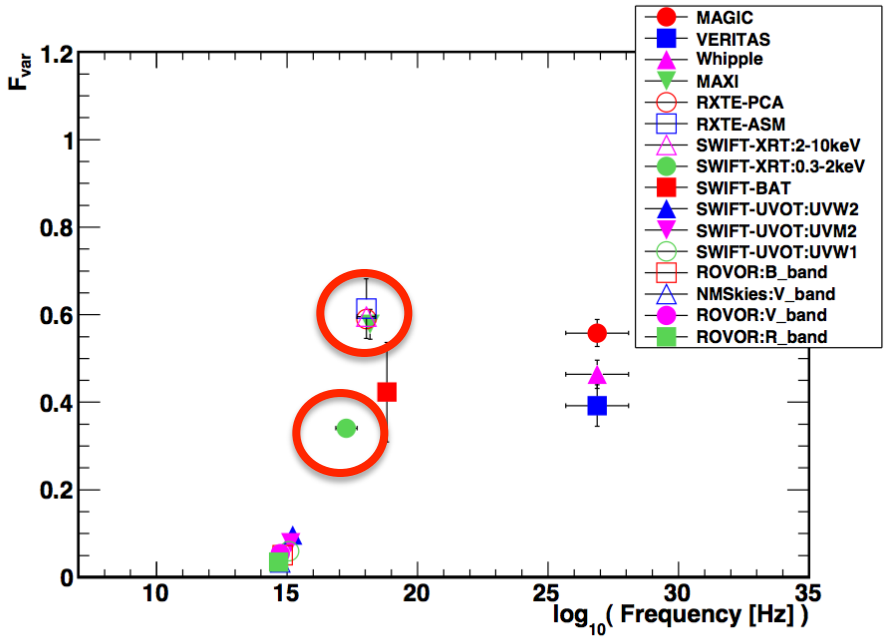

Similar behaviour observed during the non-flaring and the flaring activity of Mrk421 in the campaigns from 2009 and 2010

→ Some features get repeated over time, in high and low state (intrinsic characteristic of the source)

3.1 – Variability

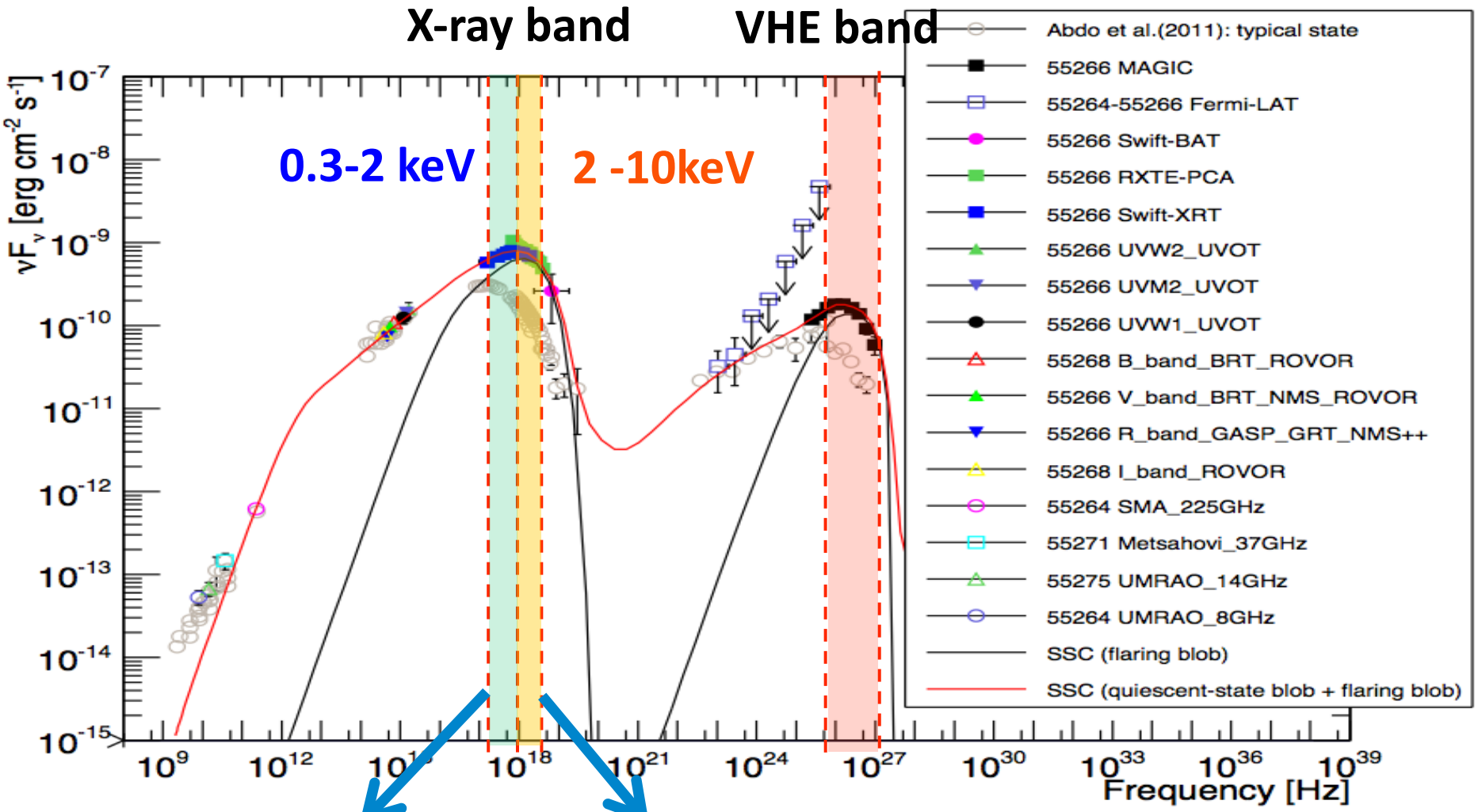

0.3-2 keV band
samples the emission
At or BEFORE the Sync. peak

2-10 keV band
samples the emission
At or AFTER the Sync. peak

3.2 – Correlations

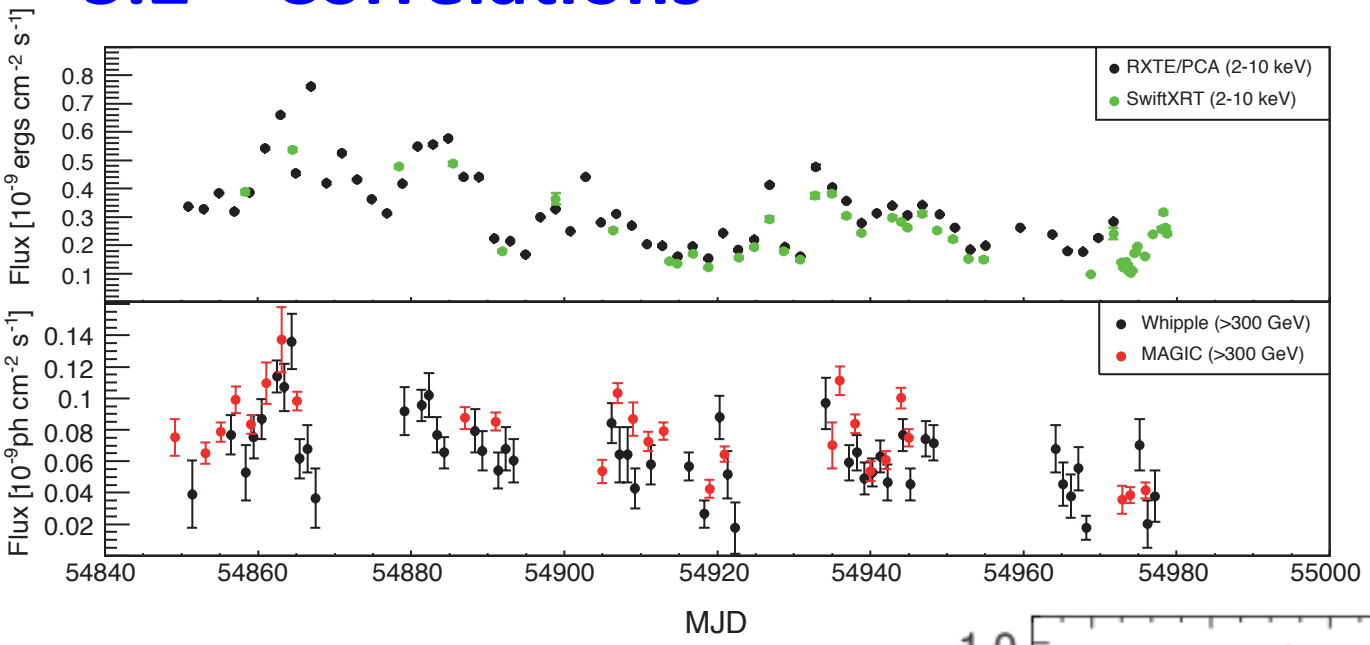

Mrk421
MW 2009

Low state and little variability in X-ray/VHE (no flares !!)

X-ray and VHE are correlated ALSO on long-term timescales and during the low activity (no flaring activity)

→ Similar processes during flaring and non-flaring activity

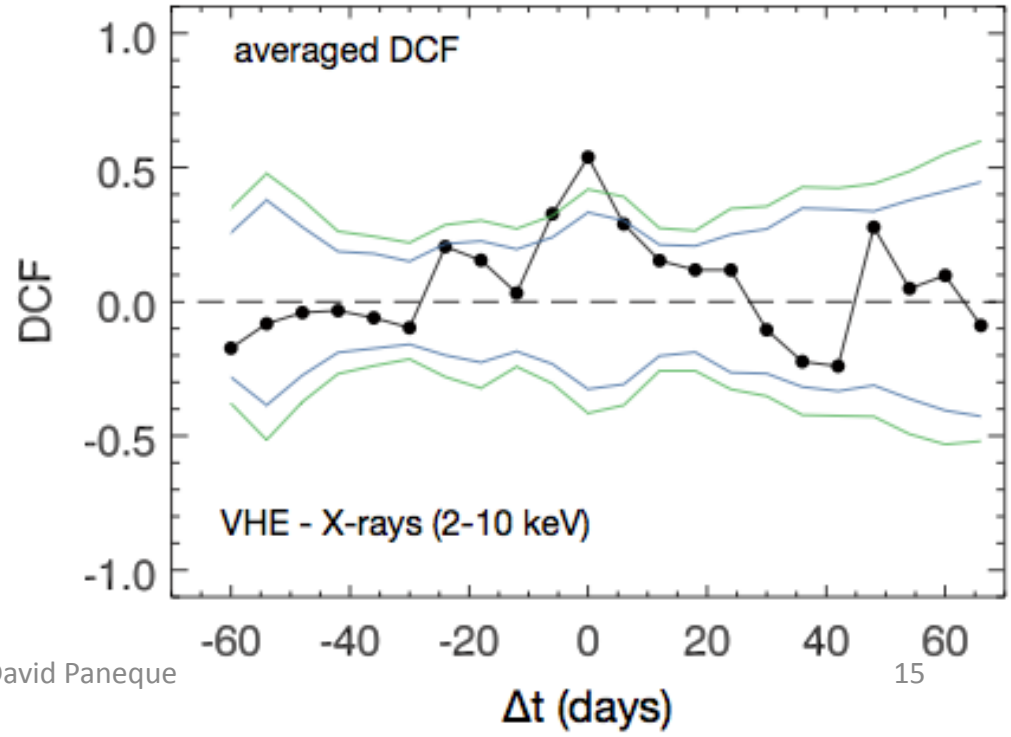

3.2 – Correlations

Correlation between radio (VLBA 43 GHz) and gamma (>0.1 GeV) also detected for Mrk421 during non-flaring (but variable !!) activity

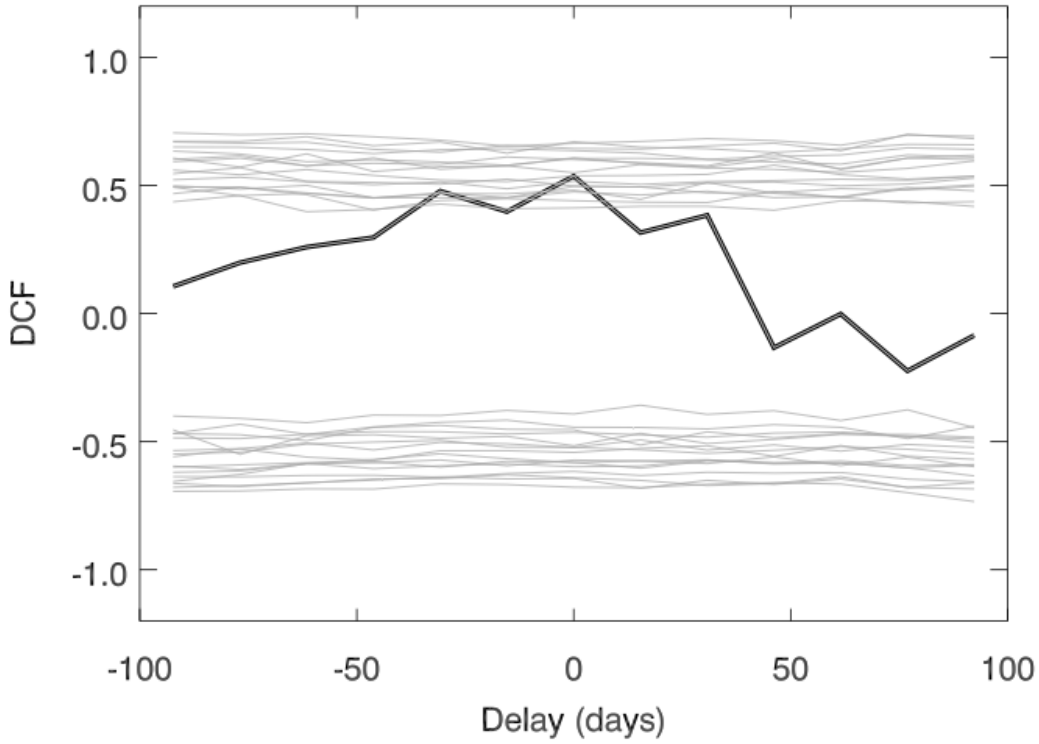

See further details in the poster 8.12, from Marcello Giroletti

Fig. 7. Discrete cross-correlation function between the γ-ray and the 43 GHz radio light curves (black curve). The gray curves represent the 99.7% confidence limits relative to stochastic variability, obtained from the combination of different power spectral density slopes. See section 3.5 for more details.

3.2 – Correlations

Correlations
Radio/Gamma
X-ray/TeV
observed on months timescales, non-flaring activity

→ Favor leptonic scenarios

Hadronic scenarios cannot explain this persistent correlation (radio/gamma and X-ray/VHE) during non-flaring activity and long timescales

An hadronic component is not excluded, but it cannot dominate the overall broadband variability

3.3 – SED modeling

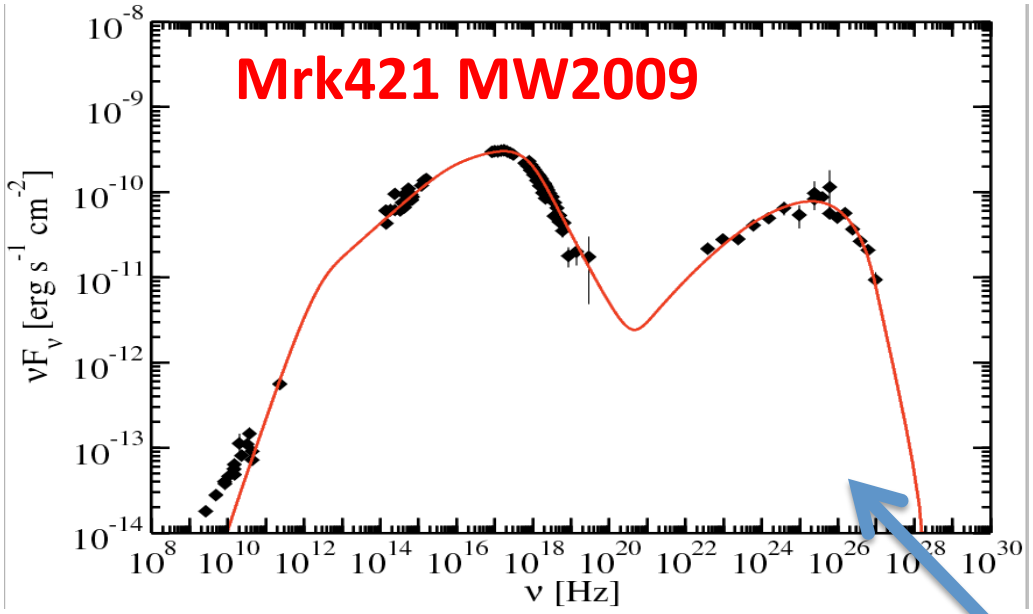

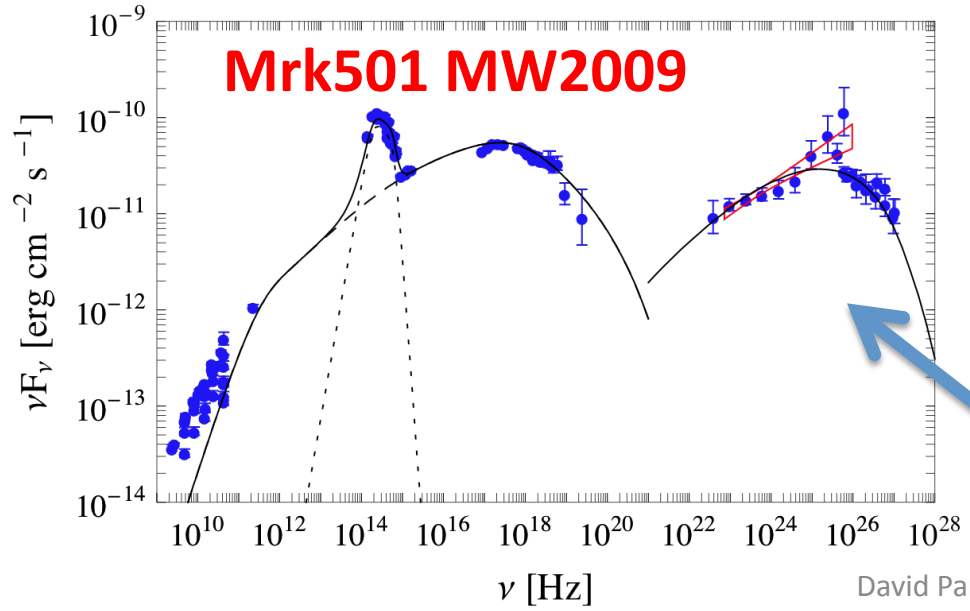

One-zone SSC describes well the broadband (radio to VHE) data collected for Mrk421 and Mrk501 during non-flaring activity

→Done many times in the past, but with less temporal and energy coverage.
First time with Fermi-LAT !!

Abdo et al., ApJ 736 (2011) 131

Abdo et al., ApJ 727 (2011) 129

3.3 – SED modeling

One-zone SSC also describes well the broadband (radio to VHE) data collected for Mrk421 when it flares

→ **Done many times in the past, but with less temporal and energy coverage**

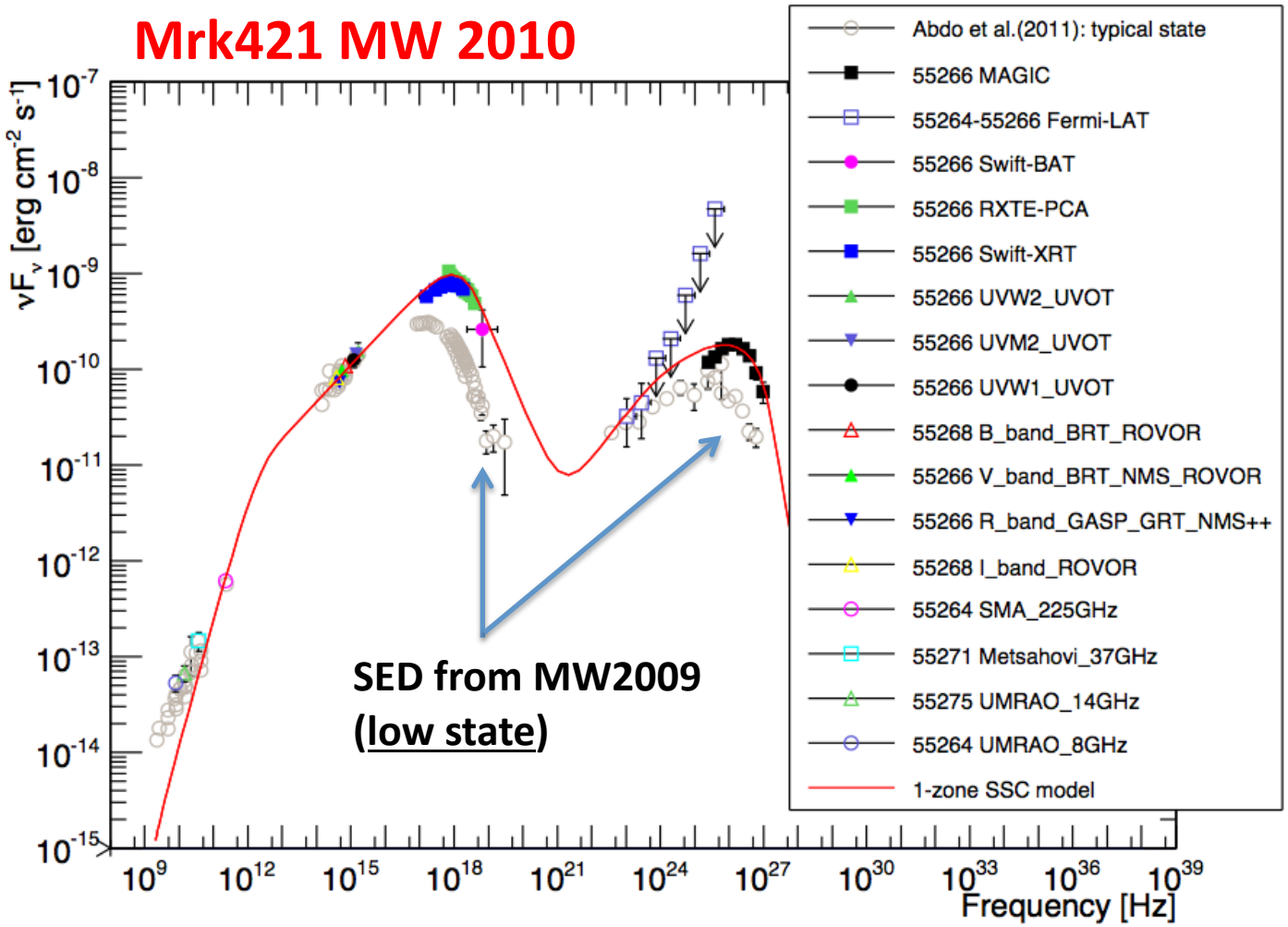

See backup slides for the SED modeling during the flaring activity monitored during 13 consecutive days, and also for the parameter values retrieved from the models

3.3 – SED modeling

We also successfully modeled the SED with a <u>two-zone SSC</u>
→ quiescent + flaring (essentially only in X-ray and VHE)

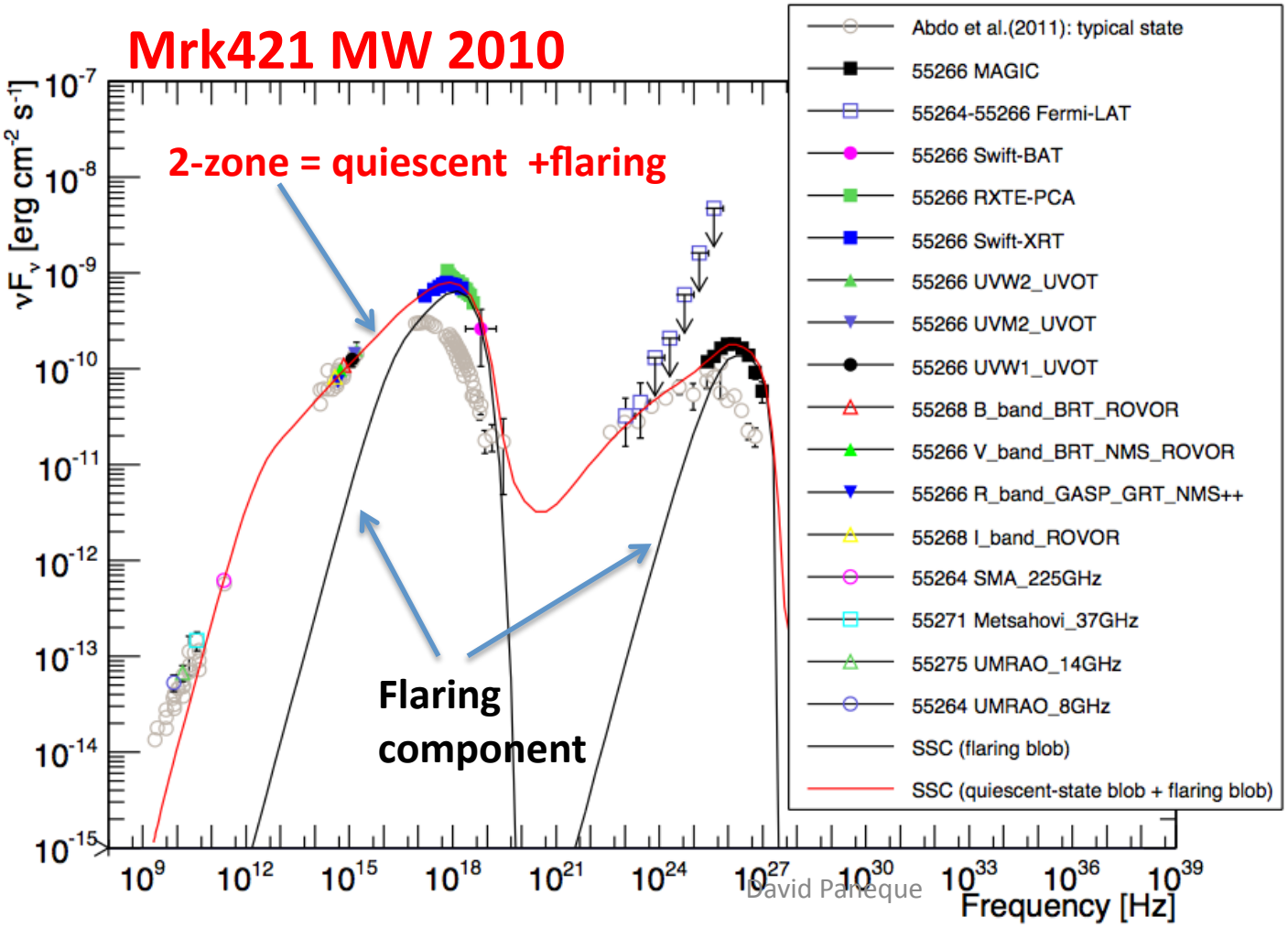

See backup slides for the SED modeling during the flaring activity monitored during 13 consecutive days, and also for the parameter values retrieved from the models

3.3 – SED modeling

One-zone vs two-zone SSC model

→ Both of them provide reasonably good agreement

→ Two-zone SSC describes slightly better the narrow peaks

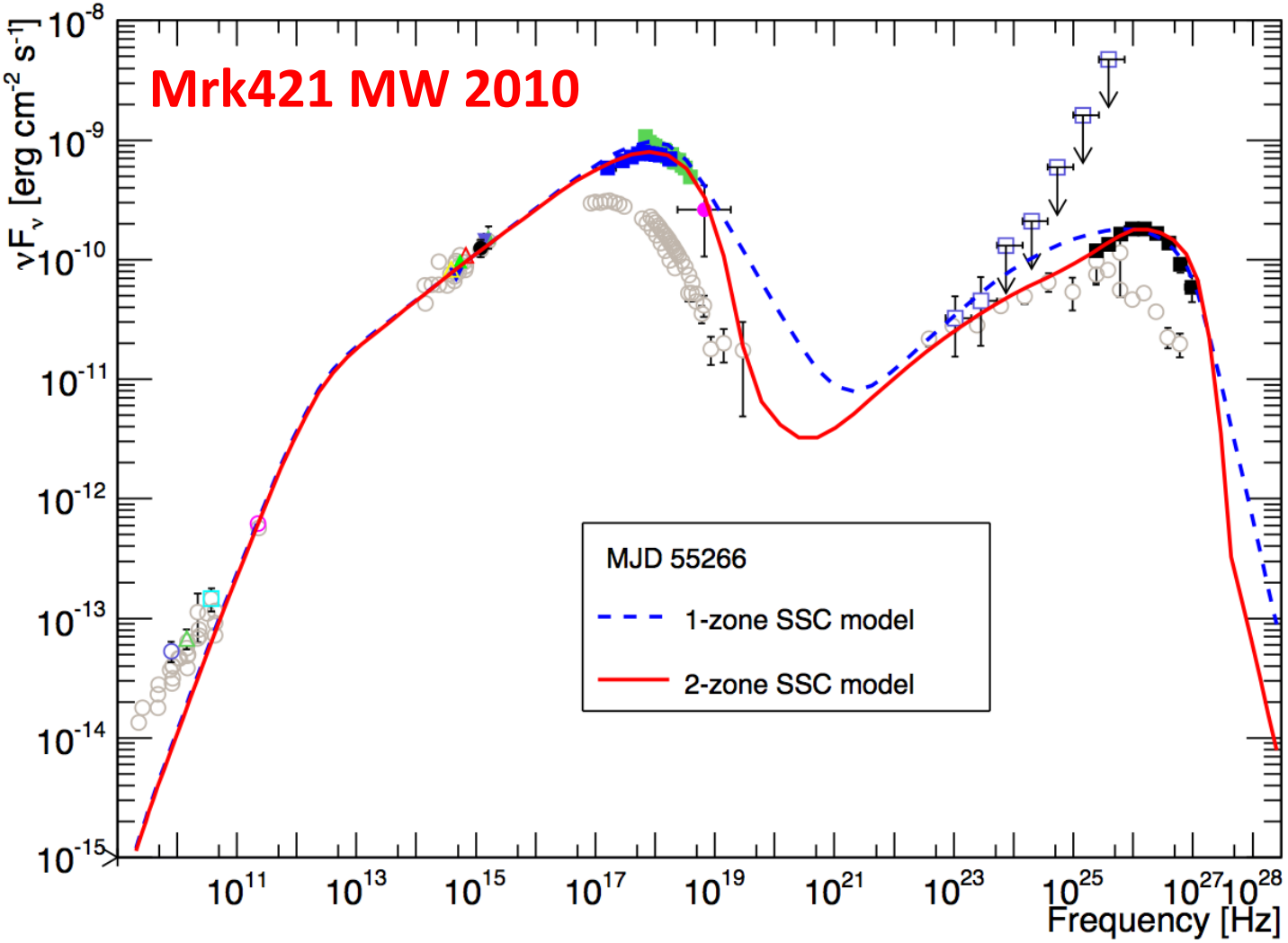

3.3 – SED modeling

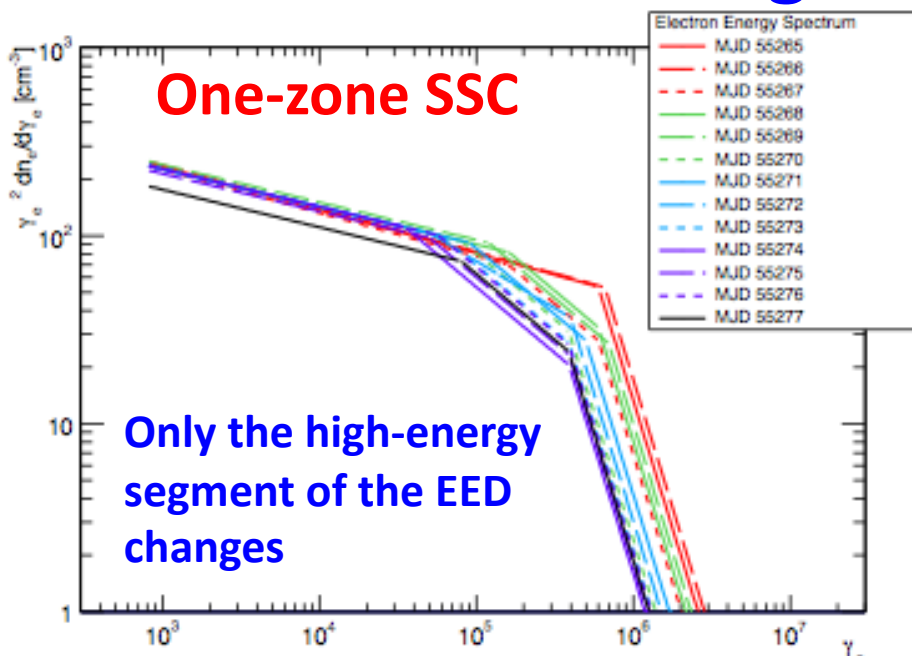

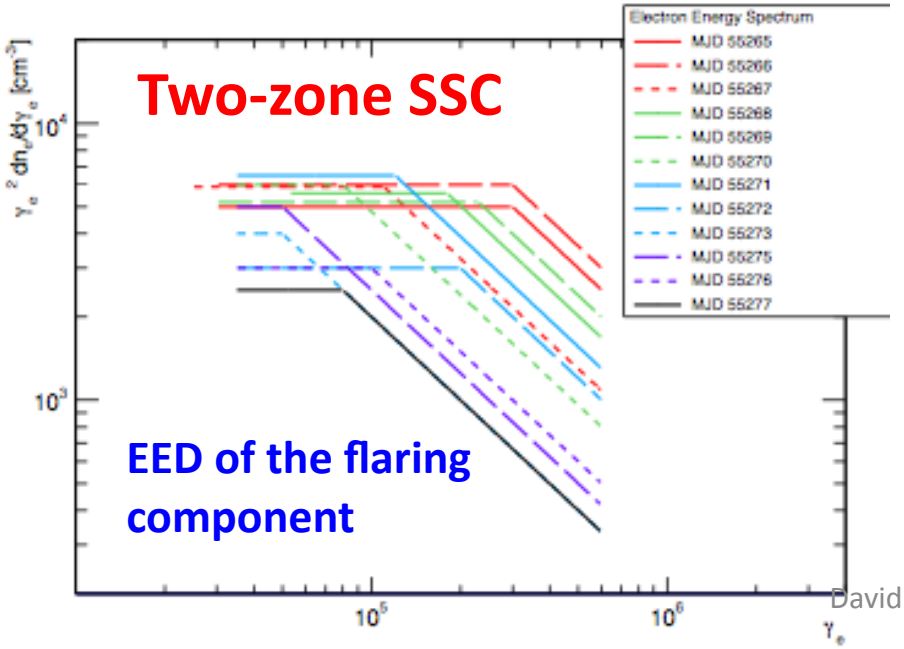

Mrk421 MW 2010

One-zone vs two-zone SSC model

In both cases we could describe the 13-day long flaring activity with changes in the electron energy distribution (EED)

Variations in the broadband SED during the flaring episodes in blazars may be dominated by particle acceleration-and-cooling

3.4 - Flaring activity with EVPA rotation

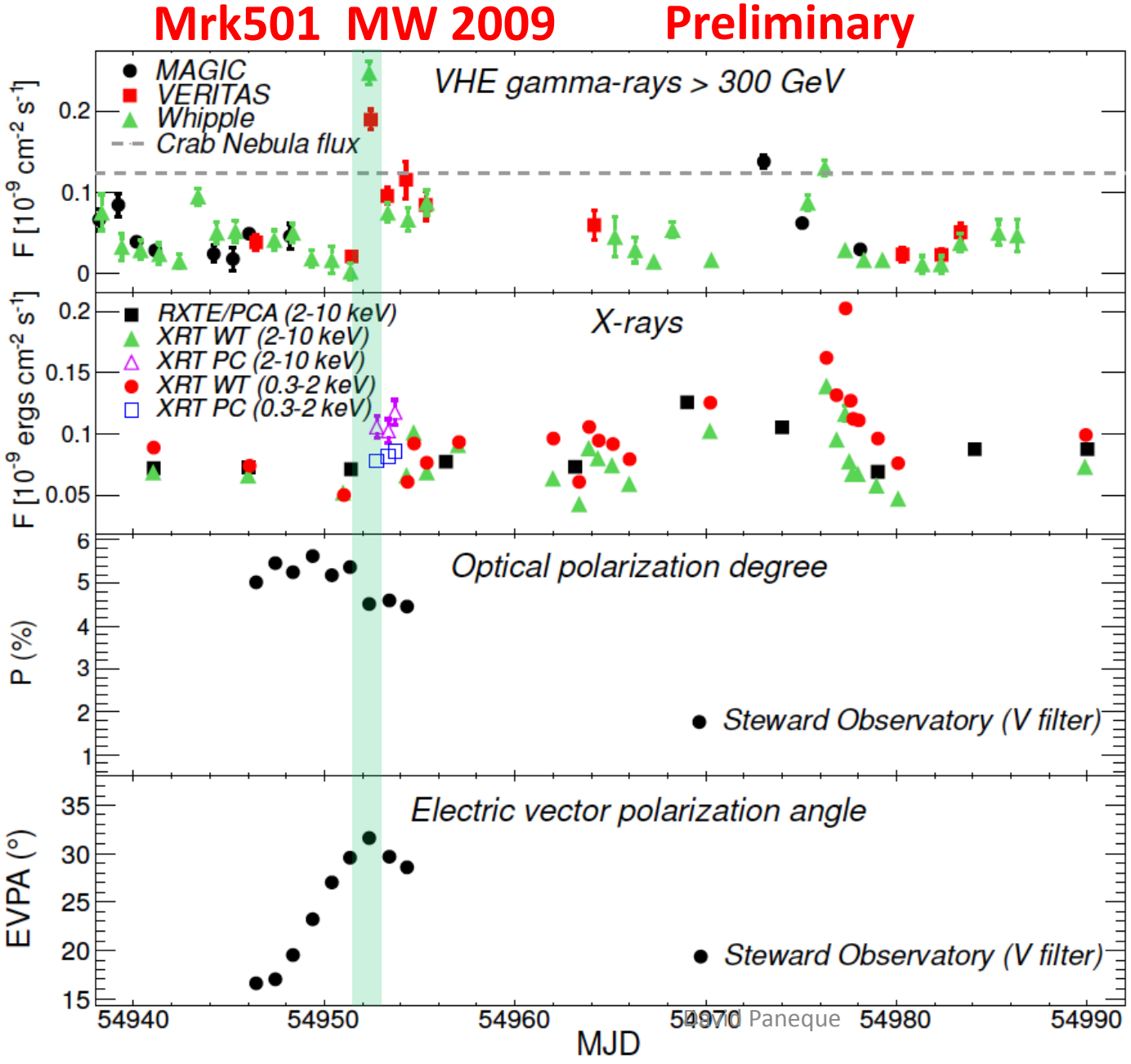

Rotation of EVPA that stops right at the day of the big TeV flare

NEVER observed before for Mrk501

3.5 – Flaring activity with ejection of VLBA blobs

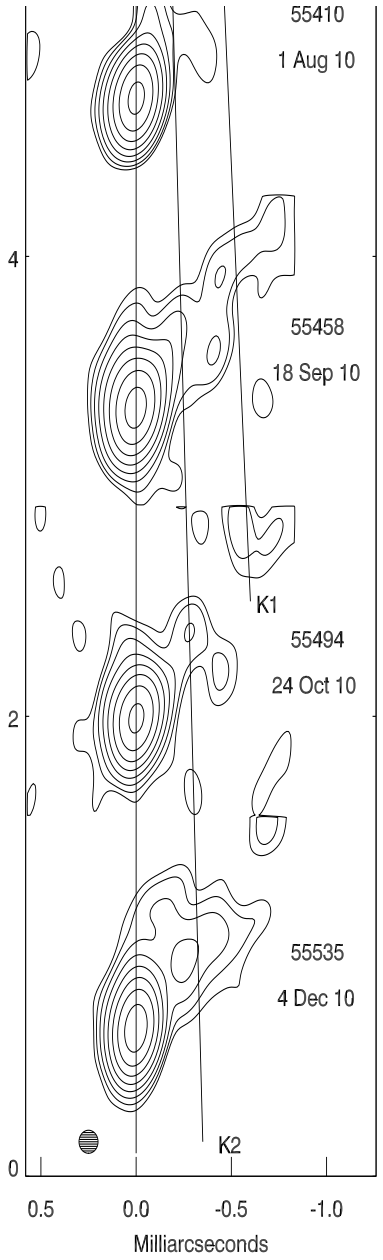

Mrk421 is also monitored with VLBA by the Boston Univ. Blazar group

VLBA components K1 and K2 traced back to the VLBA core in January and March 2010, coinciding with the flaring activities in 2010 January and March (but NOT with the BIG Flare in February)

Correlation between flaring activity and "ejection" of VLBA blobs
NEVER seen before for Mrk421

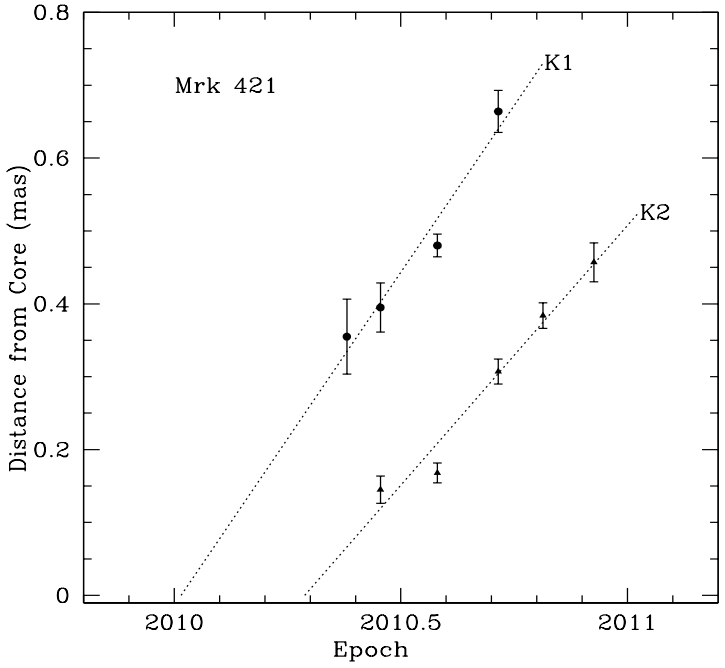

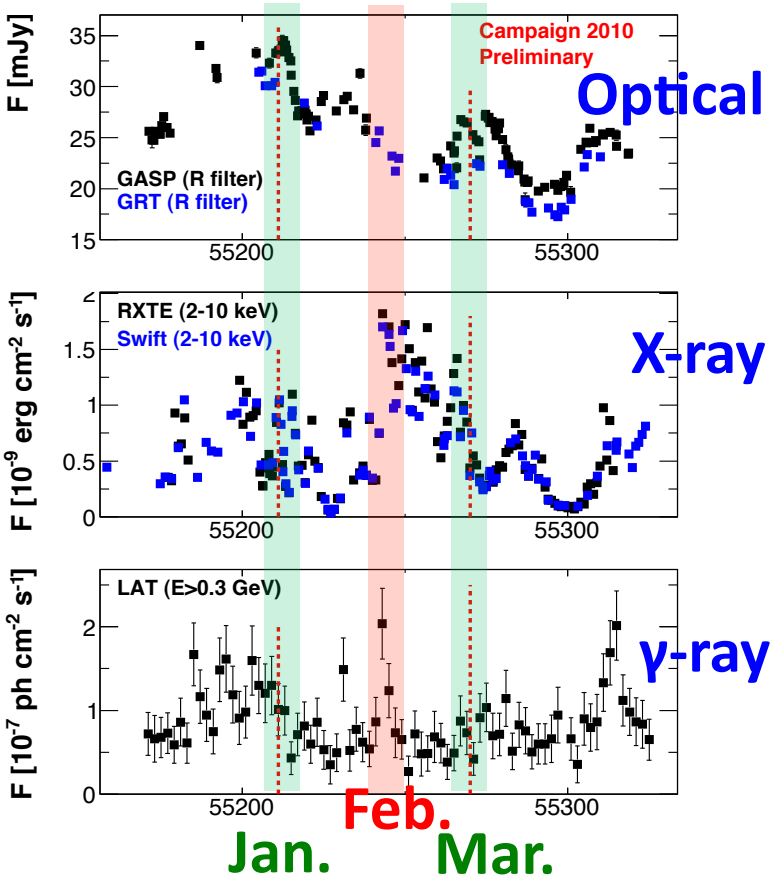

Flaring activity with EVPA rotation
+
Flaring activity with ejection of VLBA blobs

Similar (but not identical !!) behaviour observed for various other sources (LBLs and FSRQs) in the last years:

BL Lacertae : Marscher et al, Nature 452 (966), 2008
PKS 1510-089 : Marscher et al, ApJL, 710 (126), 2010
3C 279 : Abdo et al, Nature 463 (919), 2010
3C 454.3 : Jorstad et al, ApJ 715 (362), 2010
OJ 287 : Agudo et al, ApJ 726 (13), 2011
AO 0235+164 : Agudo et al, ApJ 735 (10), 2011

NEVER observed before for Mrk421, Mrk501 or any other HBL

→ similar physical processes occur in jets of different blazar subclasses
(which have different apparent jet speeds and overall power outputs).

Some flares may occur in the "acceleration and collimation region"
(highly ordered B field)

Other flares may occur in the "quasi-stationary VLBA core"
(turbulent B field, 1-100 pc downstream the supermassive black hole)

4 – Conclusions

The MW campaigns on Mrk421 and Mrk501 are a multi-year AND multi-instrument program that is running since 2009.

Deepest Temporal and Energy coverage on any TeV object

→ *Many interesting (novel) results, and many more to come*

We can use Mrk421 and Mrk501 as our blazar physics laboratory

Lessons learnt might be applied to other blazars (farther away or weaker)

Large complexity in the temporal evolution of the broadband (radio to VHE γ-rays) SED.

→Lots of things to learn….

Backup

3.6 - Constrains on EBL density

Slide from Franceschini

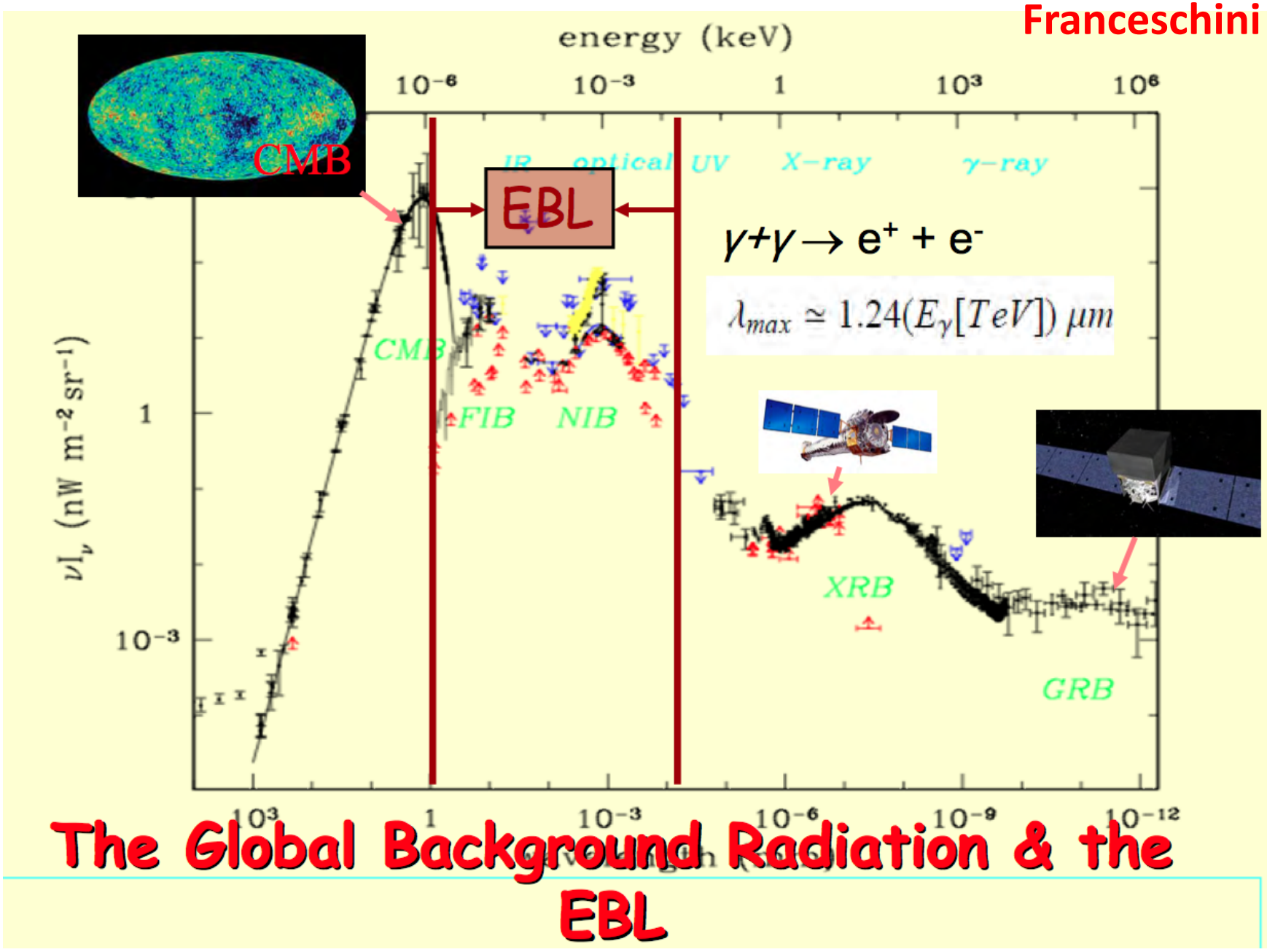

The Global Background Radiation & the EBL

3.6 - Constrains on EBL density

From Dominguez et al., 2011

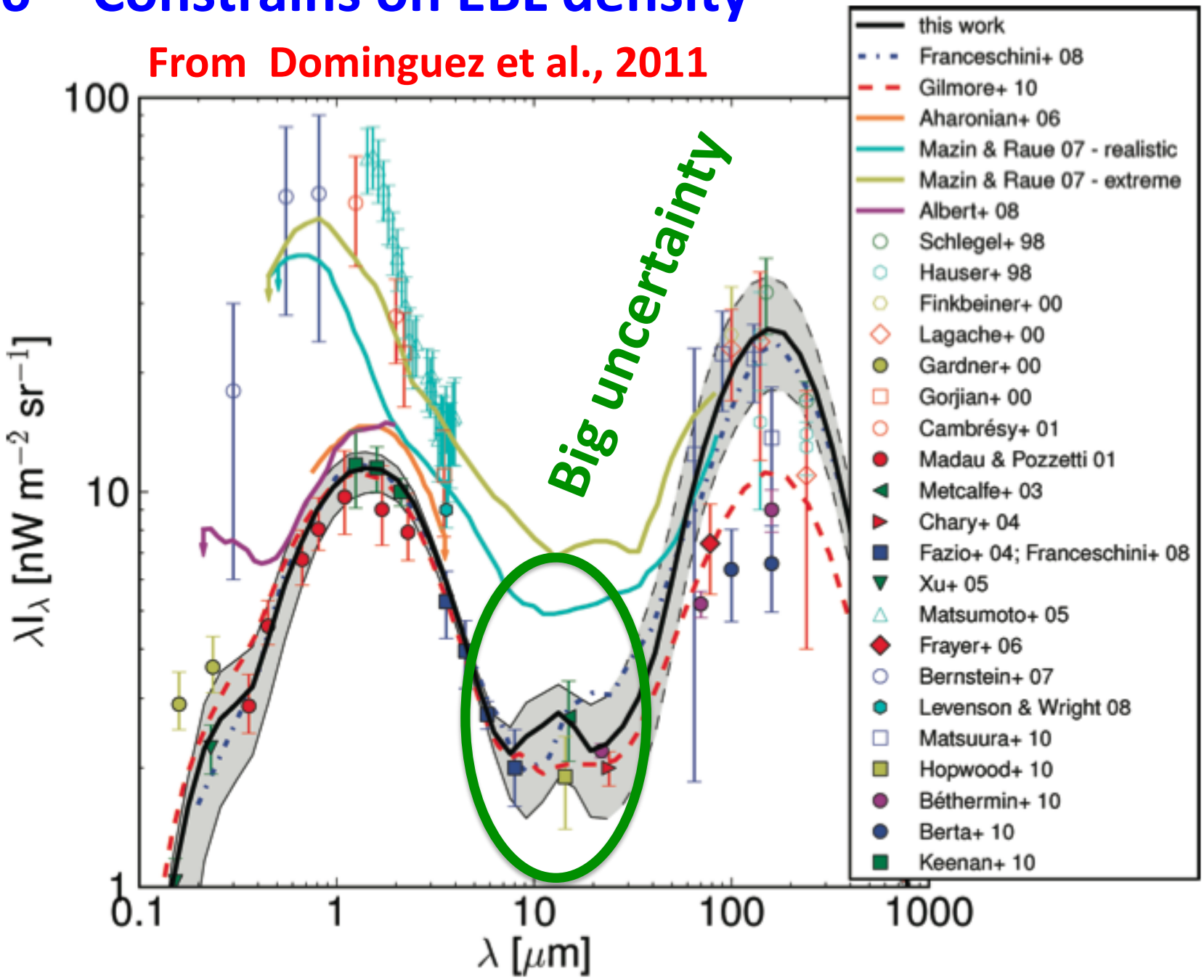

From Dominguez et al., 2011

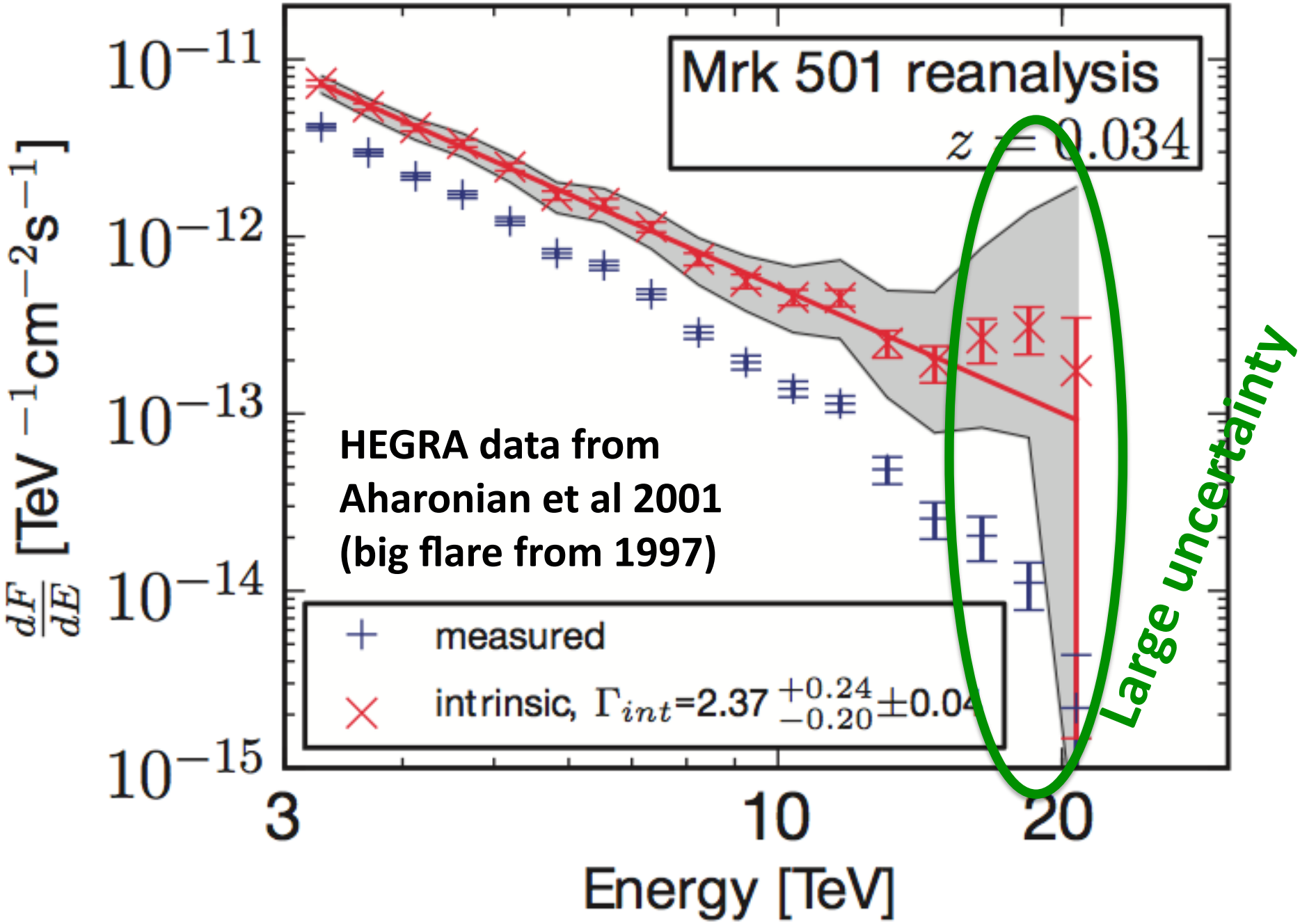

3.6 - Constrains on EBL density

On February 17th, 2010, Mrk421 showed outstanding flaring activity. VERITAS observed Mrk421 for more than 5 hours, and detected a peak flux of ~12 Crab units, although without large intra-night variability

Mrk421 MW2010 (VERITAS Light curve for February 17th)

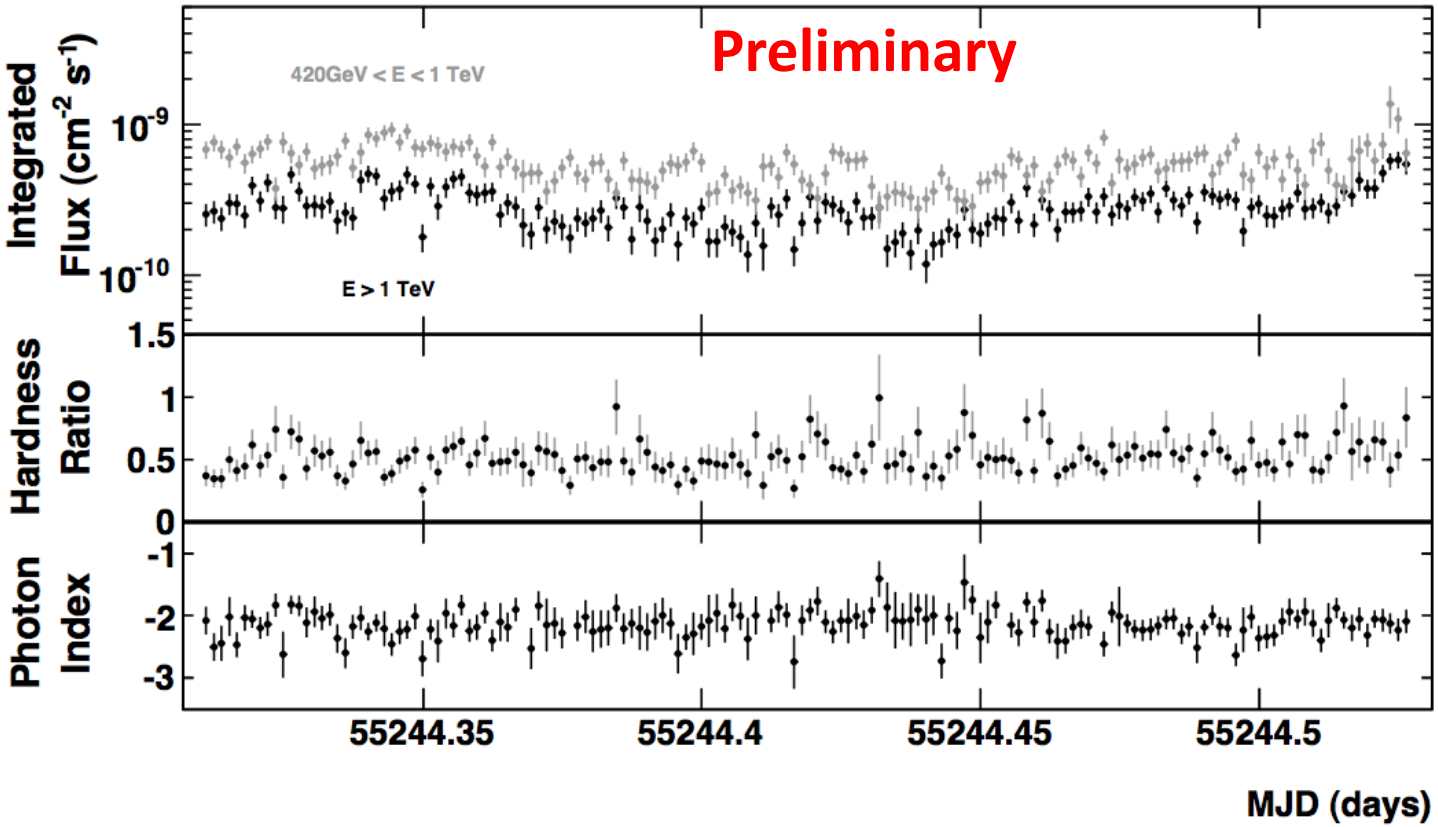

3.6 - Constrains on EBL density

The Mrk421 flare delivered photons above 10 TeV, which nominally allows to set constrains to the EBL density beyond 10 microns

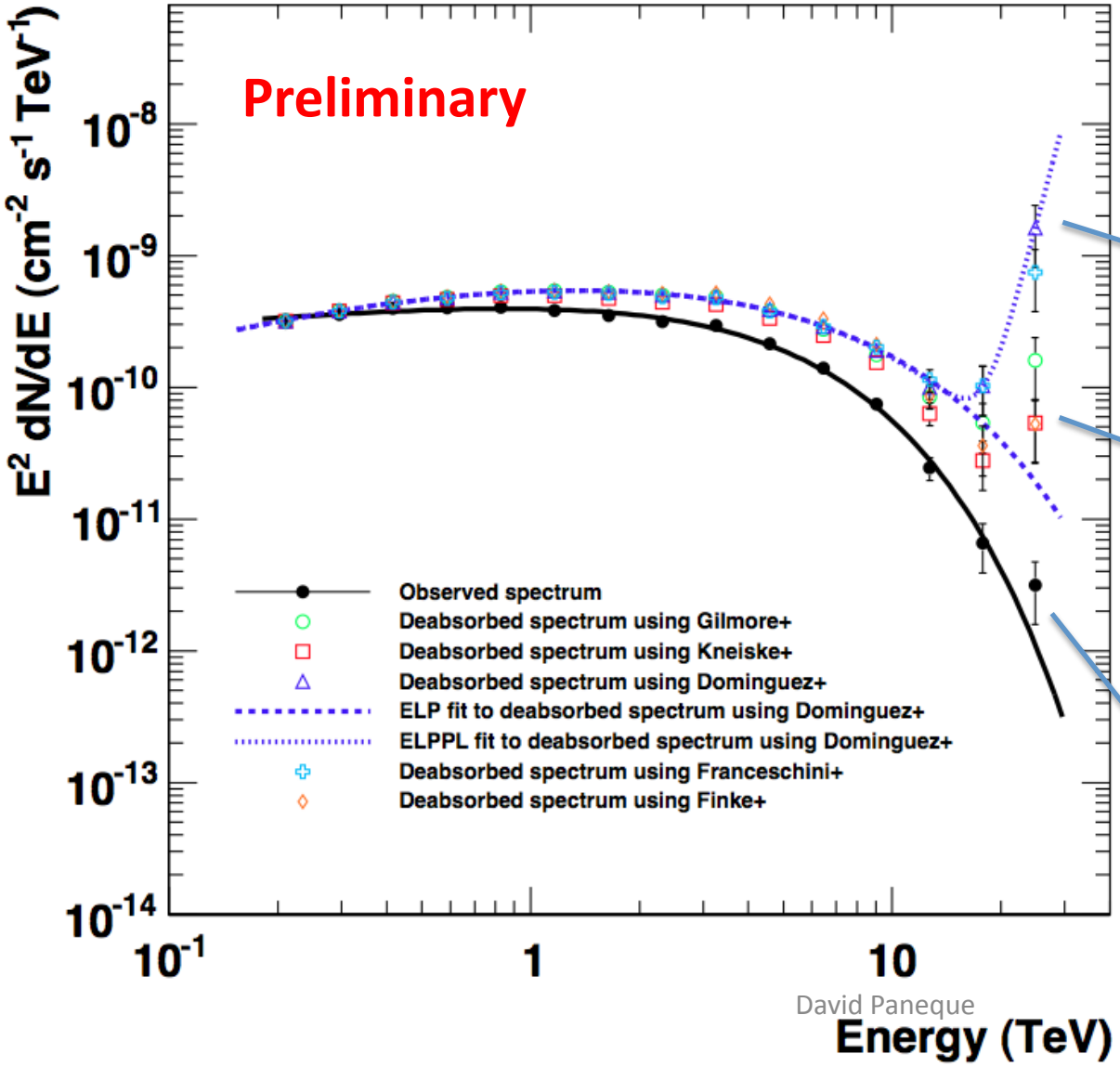

$$\lambda_{Peak} = 1.24\left(E/_{TeV}\right)\mu m$$

Deabsorbed with EBL Dominguez at al 2011

Deabsorbed with EBL Kneiske at al 2004 (low)

Observed spectrum Highest point @25 TeV (3.5 sigma)

3.6 - Constrains on EBL density

Large differences data-model above 15 TeV

→ Model is a log-parabola with EBL correction

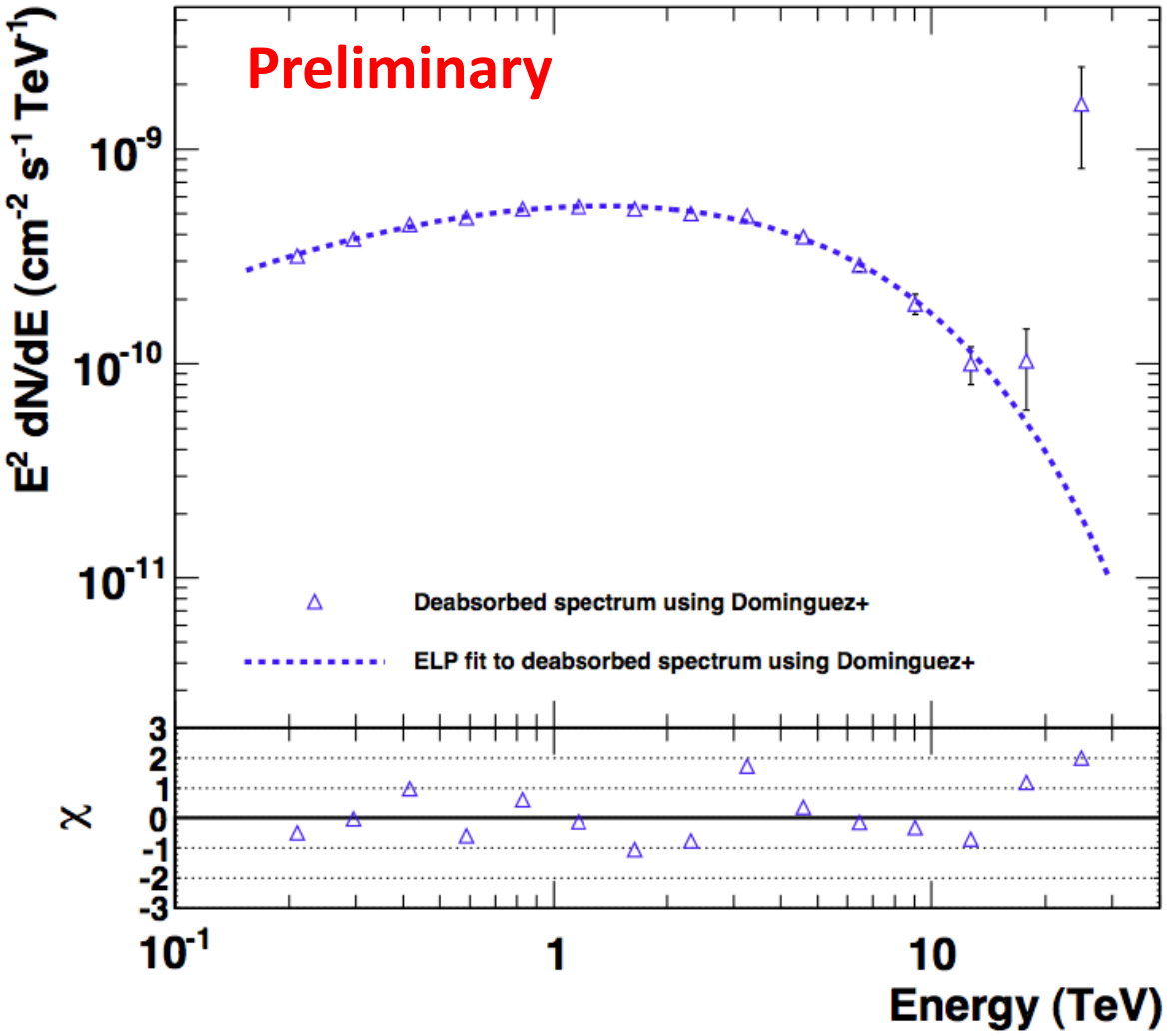

Deviation data-model above 20 TeV is ~2 orders of magnitude

But only at 2 sigma significance due to the large statistical error in the flux measurement

→ Large statistical error is unavoidable because of low-photon statistics @25 TeV: only 5 photons !!

SED modeling (Mrk421, 2010 March flare)

Very good simultaneity in MW observations

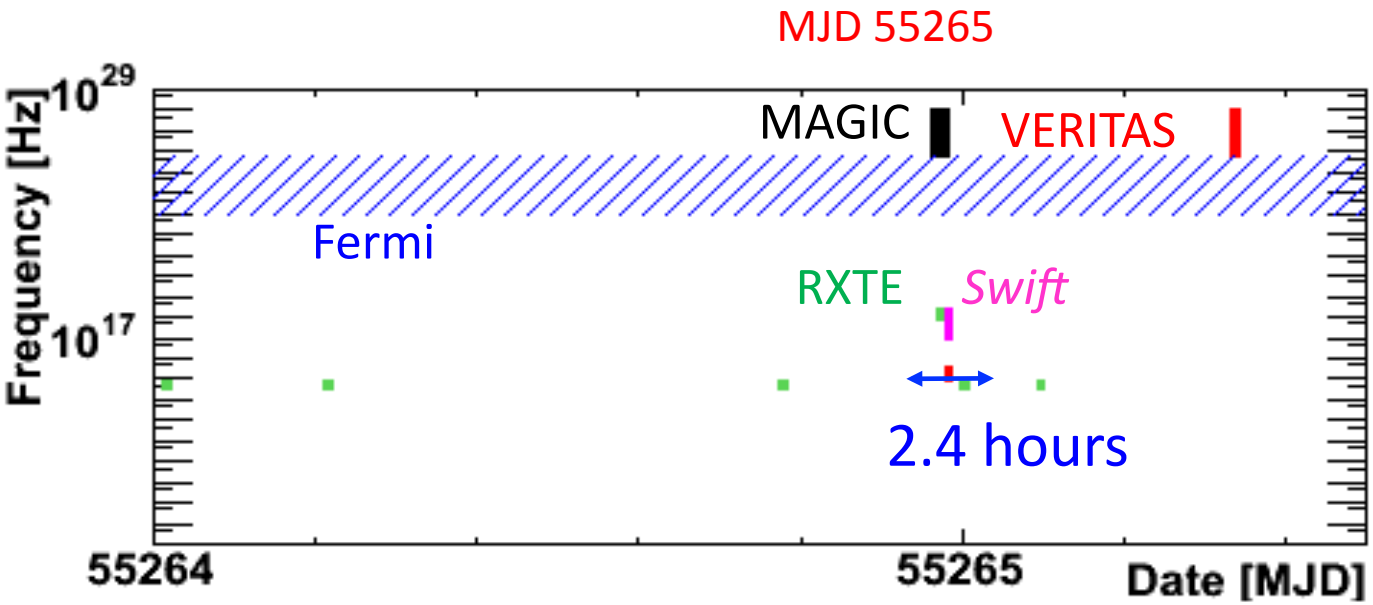

Observations are truly simultaneous

→ Very important during flaring activity

→ reliability in the results derived with these data

We can study the evolution of the SED during 13 consecutive days

Mrk421, flaring activity from March 2010

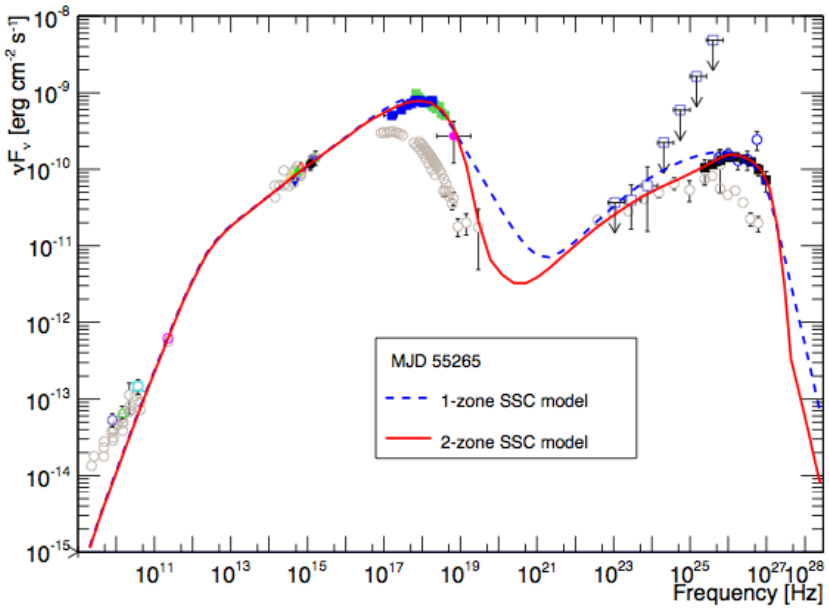

(a) MJD 55265.

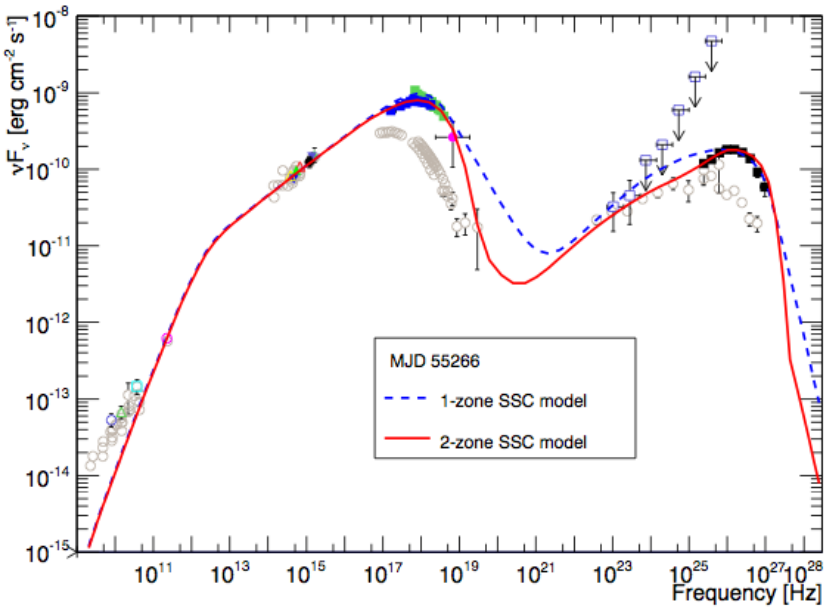

(b) MJD 55266.

Fig. 15: Broadband SEDs from MJD 55265 and 55266 (the two days with the highest activity) with the one-zone and two-zone model curves described in sections 4.2 and 4.3. Refer to Figures 7 and 8a for details of the data points.

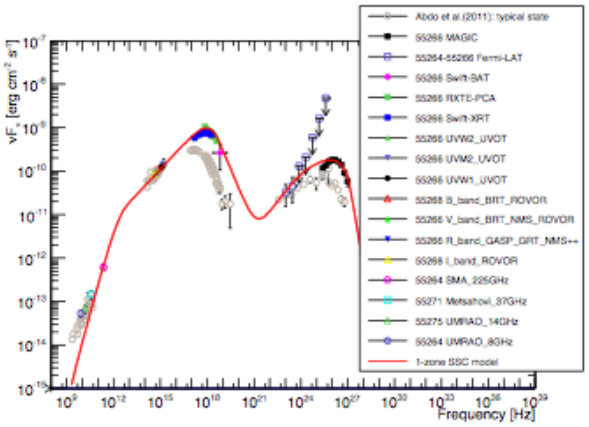

(a) MJD 55266.

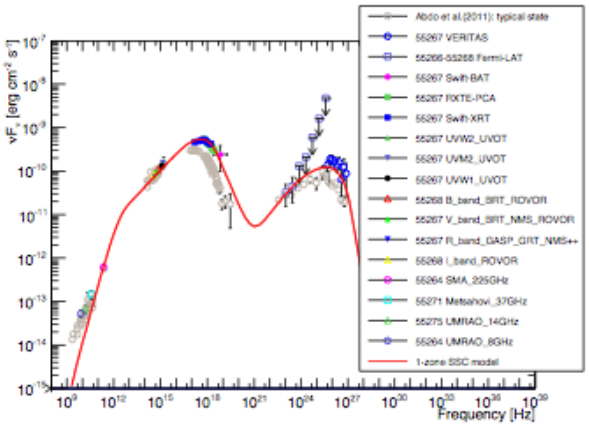

(b) MJD 55267.

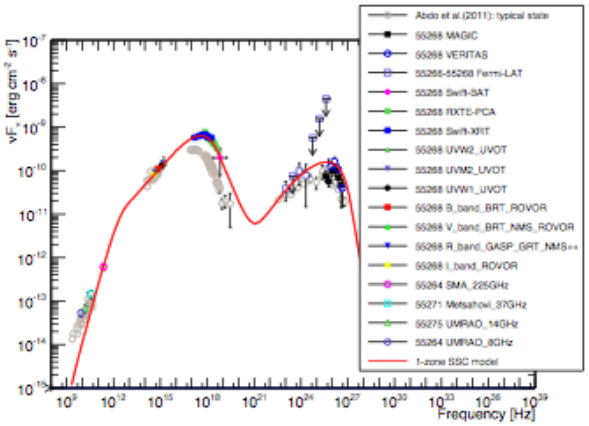

(c) MJD 55268.

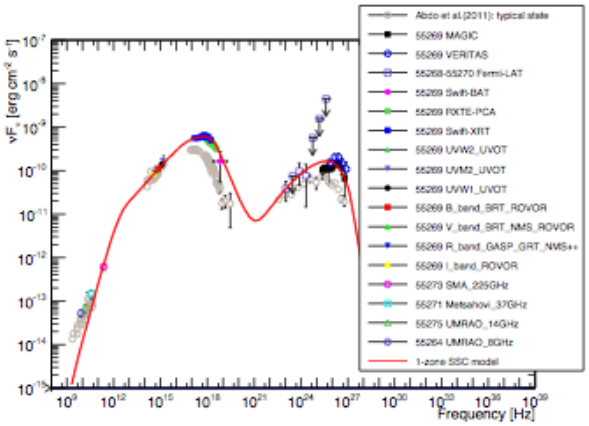

(d) MJD 55269.

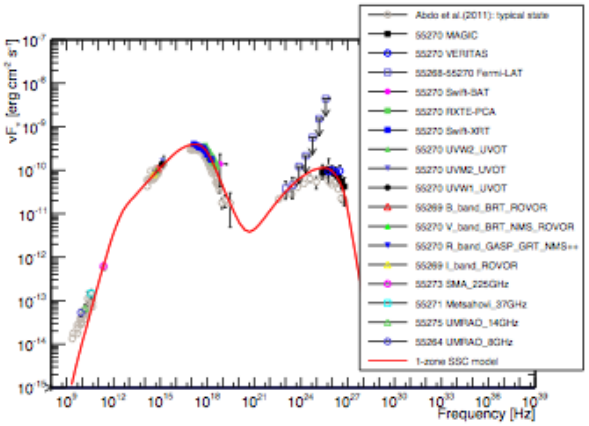

(e) MJD 55270.

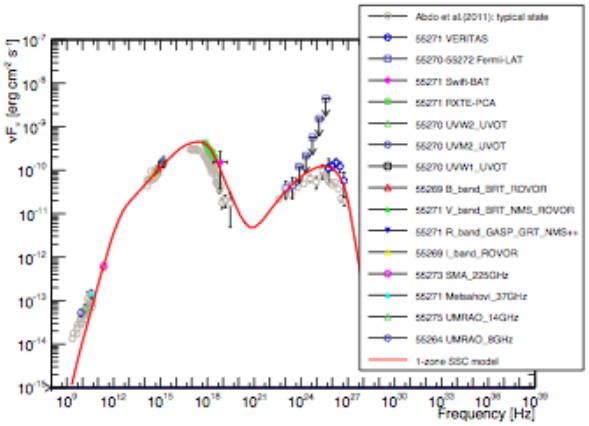

(f) MJD 55271.

Mrk421 13-day long flaring activity during March 2010

Broadband SEDs measured on single days can be described with 1-zone SSC model (Part 1)

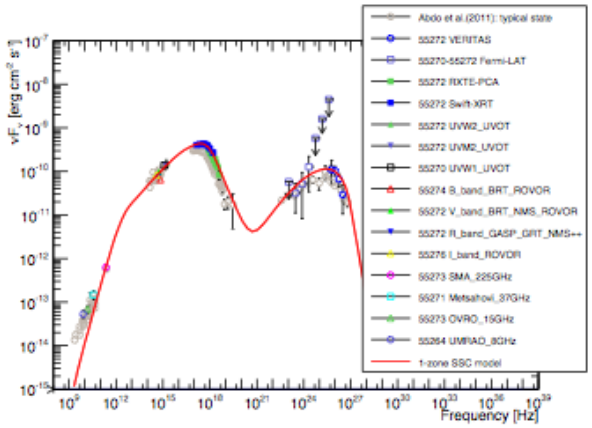

(a) MJD 55272.

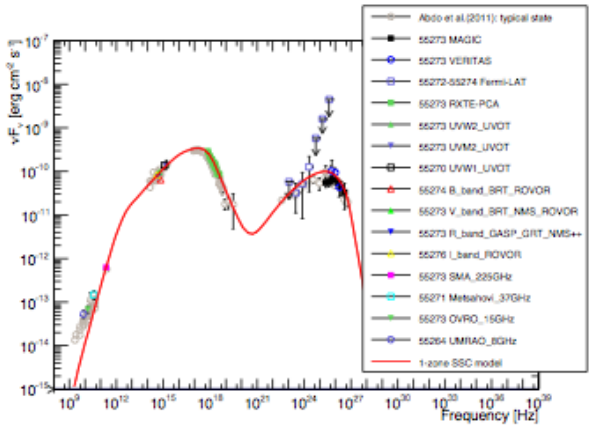

(b) MJD 55273.

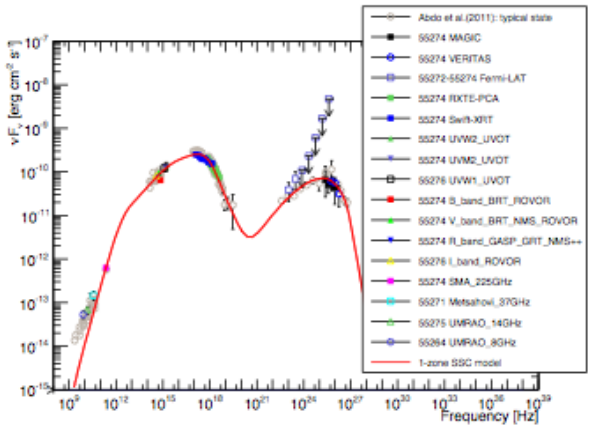

(c) MJD 55274.

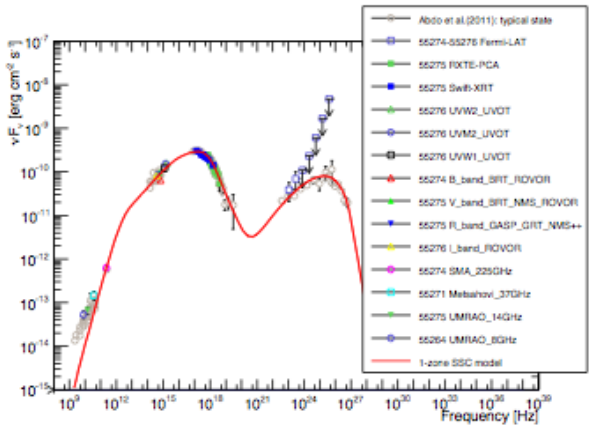

(d) MJD 55275.

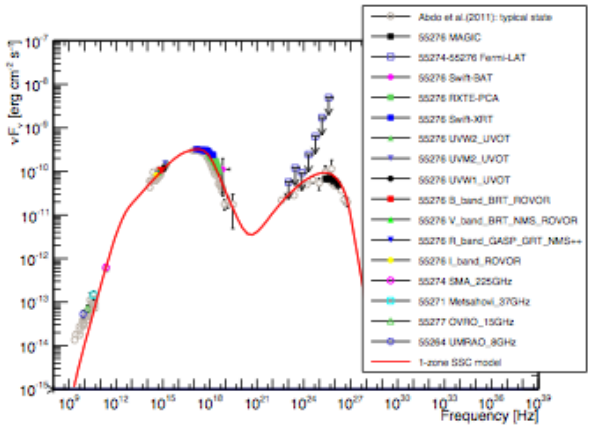

(e) MJD 55276.

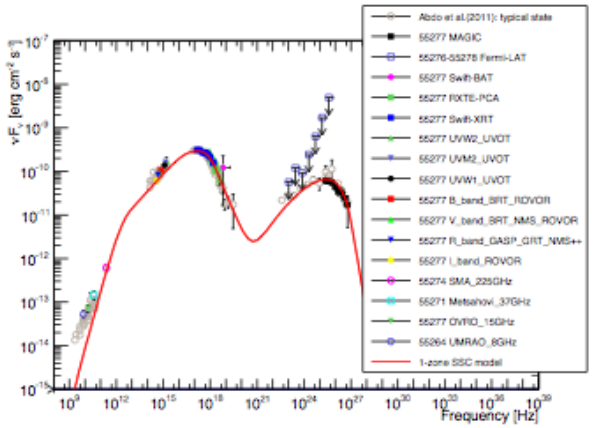

(f) MJD 55277.

Mrk421 13-day long flaring activity during March 2010

Broadband SEDs measured on single days can be described with 1-zone SSC model (Part 2)

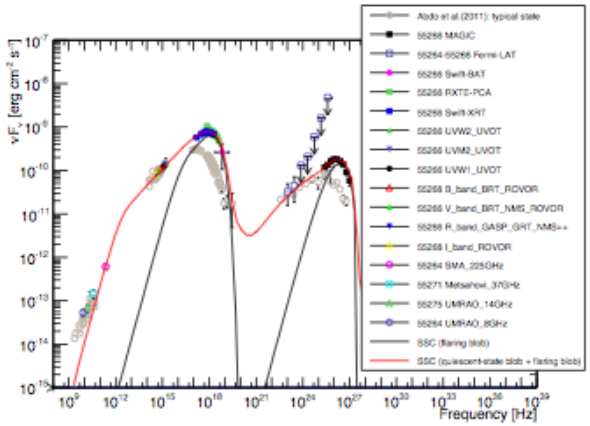

(a) MJD 55266.

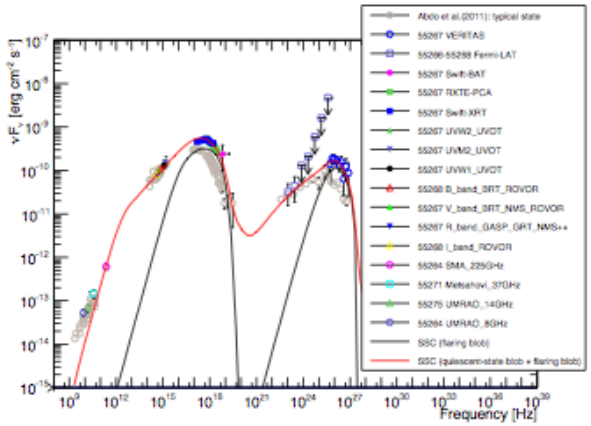

(b) MJD 55267.

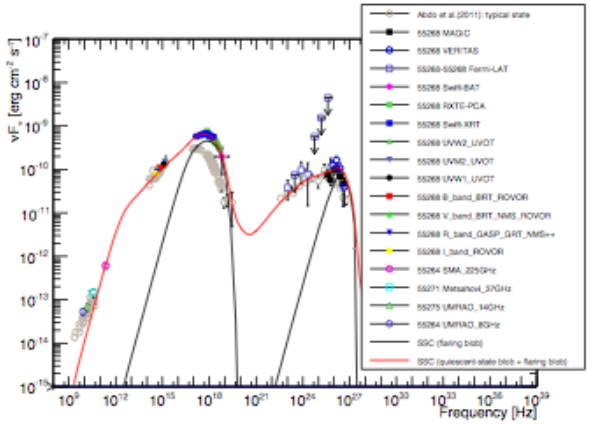

(c) MJD 55268

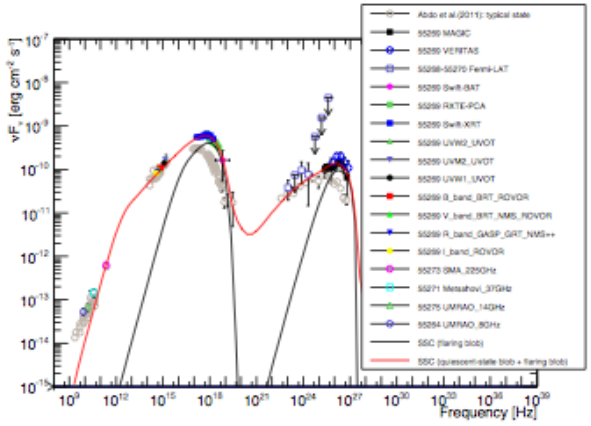

(d) MJD 55269.

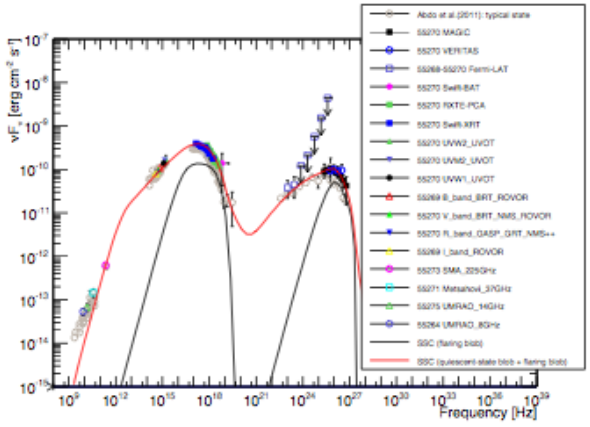

(e) MJD 55270.

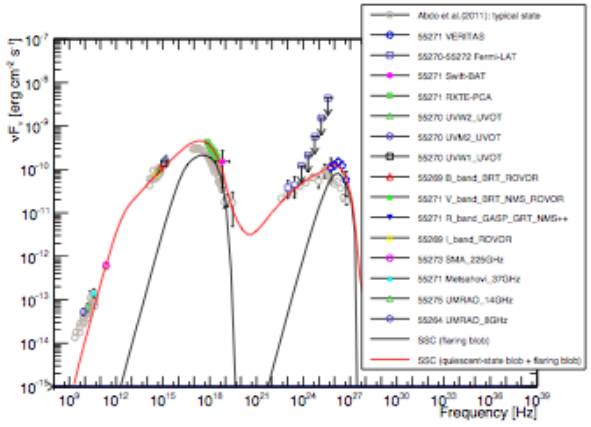

(f) MJD 55271.

Mrk421 13-day long flaring activity during March 2010

Broadband SEDs measured on single days can be described with 2-zone SSC model (Part 1)

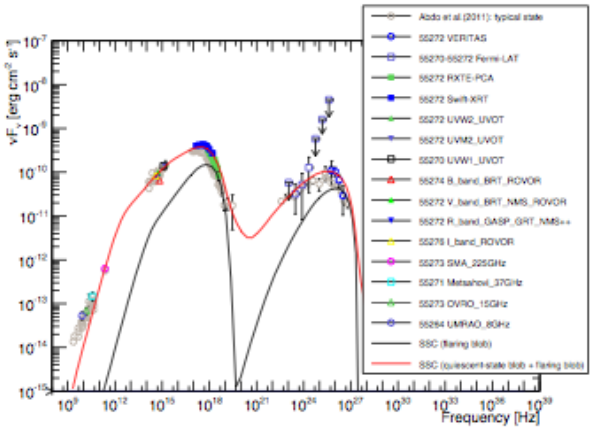

(a) MJD 55272

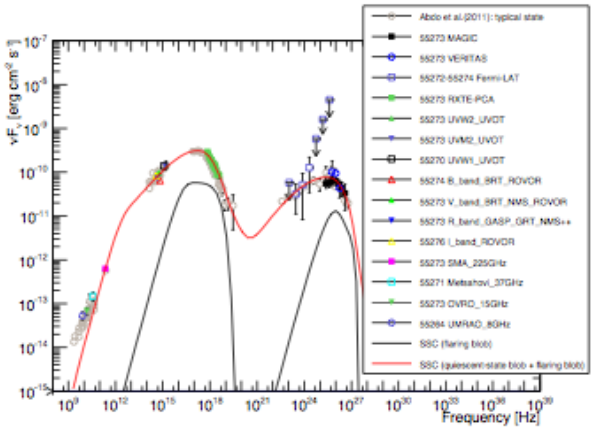

(b) MJD 55273.

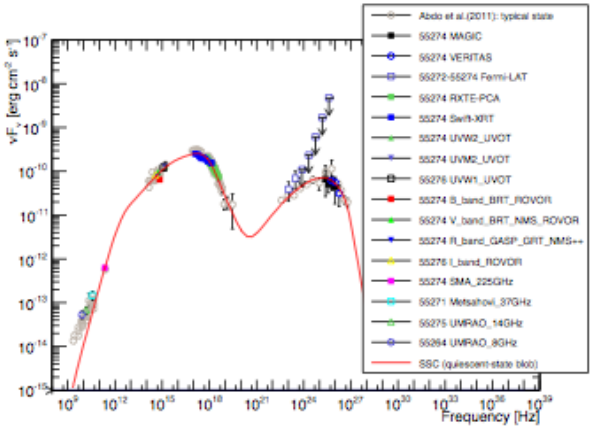

(c) MJD 55274.

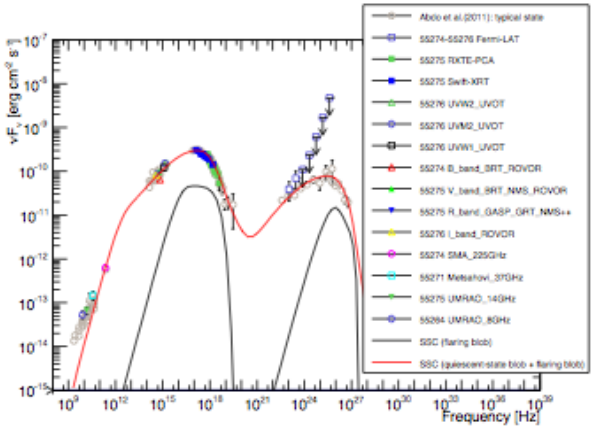

(d) MJD 55275.

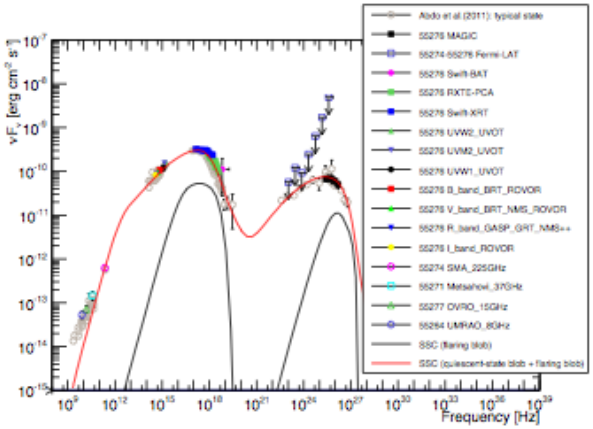

(e) MJD 55276.

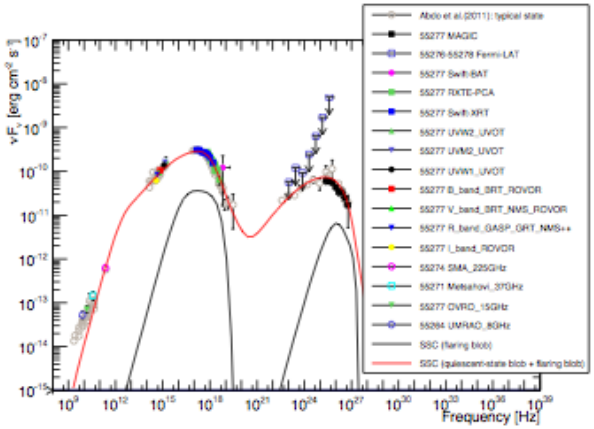

(f) MJD 55277.

Mrk421 13-day long flaring activity during March 2010

Broadband SEDs measured on single days can be described with 2-zone SSC model (Part 1)

3.3 – SED modeling

Mrk421 MW 2010

13 SEDs from models

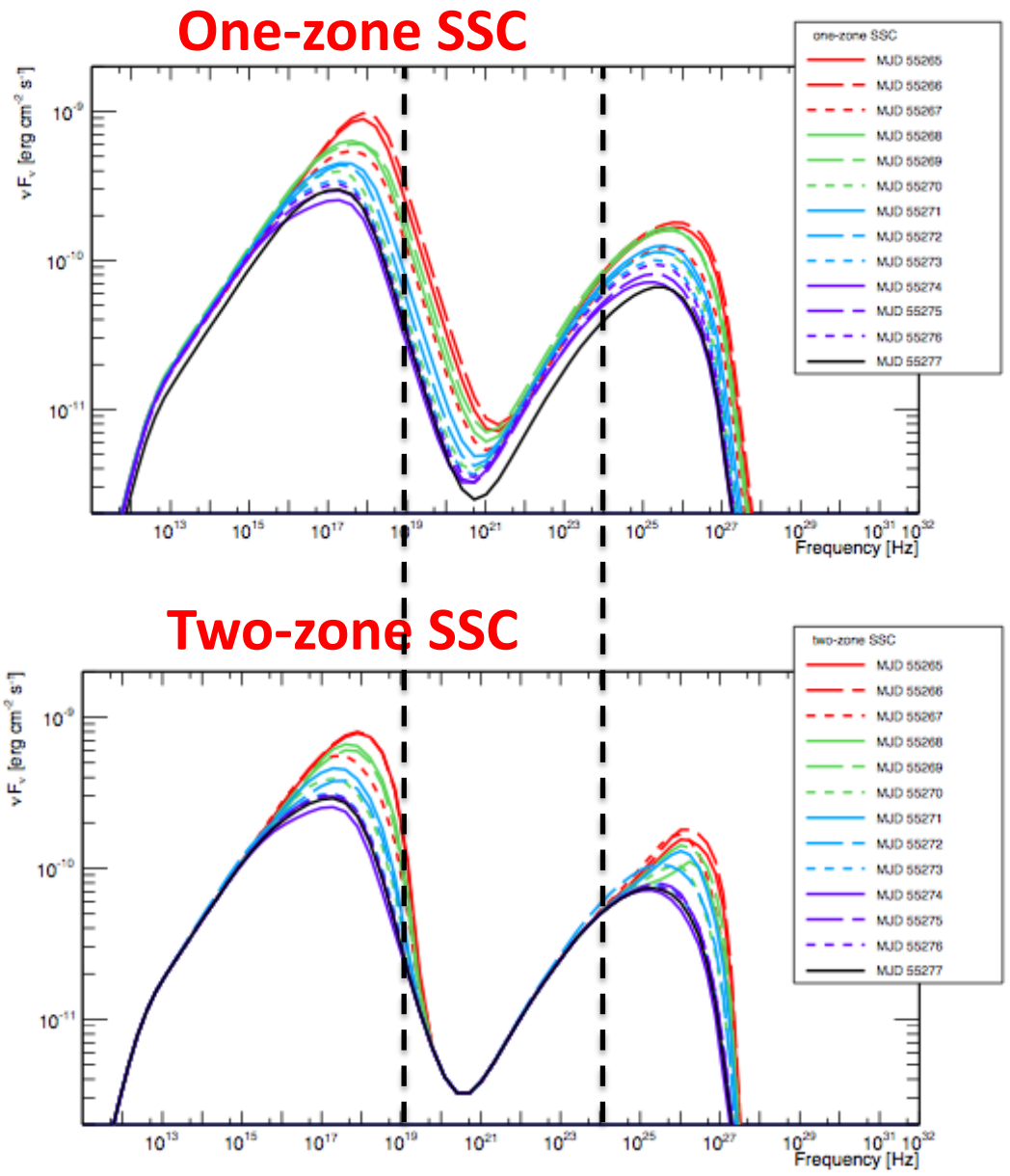

Variability patterns for the one-zone and two-zone SSC broadband emission is somewhat different, specially in the range between 50 keV and 50 GeV

The multi-band variability measured during the 13-day long flare in March 2010 could not distinguish between these two scenarios. *More prominent and longer flaring activities might make this distinction possible*

Table 2: Integral flux above 200 GeV and parameters of the one-zone SSC model. Bold-faced text is used to depict the model parameters that were varied to describe the SED during the 13-day period.

Date [MJD]	MAGIC flux [10^{-10}cm^{-2}s^{-1}]	VERITAS flux [10^{-10}cm^{-2}s^{-1}]	Whipple flux [10^{-10}cm^{-2}s^{-1}]	$\gamma_{\rm min}$ [10^2]	$\gamma_{\rm max}$ [10^8]	$\gamma_{\rm br1}$ [10^4]	$\gamma_{\rm br2}$ [10^5]	s_1	s_2	s_3	$n_{\rm e}$ [10^3cm^{-3}]	B [mG]	log(R) [cm]	δ
55265	3.8 ± 0.2	4.0 ± 0.5		8	1	**60.**	**6.0**	**2.23**	**2.23**	4.70	**1.14**	38	16.72	21
55266	4.7 ± 0.2			8	1	**66.**	**6.6**	**2.23**	**2.23**	4.70	**1.16**	38	16.72	21
55267		4.0 ± 0.5	5.3 ± 0.3	8	1	**16.**	**6.0**	**2.23**	**2.70**	4.70	**1.10**	38	16.72	21
55268	2.1 ± 0.3	4.0 ± 0.6	4.8 ± 0.3	8	1	**16.**	**6.0**	**2.20**	**2.70**	4.70	**0.90**	38	16.72	21
55269	3.3 ± 0.3	4.2 ± 0.6	4.2 ± 0.3	8	1	**12.**	**7.0**	**2.20**	**2.70**	4.70	**0.95**	38	16.72	21
55270	2.3 ± 0.2	2.6 ± 0.4	3.0 ± 0.2	8	1	**8.0**	**3.9**	**2.20**	**2.70**	4.70	**0.90**	38	16.72	21
55271		3.5 ± 0.4	4.1 ± 0.5	8	1	**9.0**	**5.0**	**2.20**	**2.70**	4.70	**0.90**	38	16.72	21
55272		2.5 ± 0.4		8	1	**5.0**	**4.0**	**2.20**	**2.50**	4.70	**0.90**	38	16.72	21
55273	1.5 ± 0.2	2.0 ± 0.4	2.5 ± 0.3	8	1	**6.0**	**3.9**	**2.20**	**2.70**	4.70	**0.90**	38	16.72	21
55274	1.0 ± 0.3	1.6 ± 0.3	1.9 ± 0.2	8	1	**3.5**	**3.9**	**2.20**	**2.70**	4.70	**0.90**	38	16.72	21
55275			1.8 ± 0.3	8	1	**5.0**	**3.9**	**2.20**	**2.70**	4.70	**0.85**	38	16.72	21
55276	1.6 ± 0.2		1.5 ± 0.3	8	1	**5.7**	**3.9**	**2.20**	**2.70**	4.70	**0.90**	38	16.72	21
55277	1.2 ± 0.1		1.4 ± 0.4	8	1	**8.0**	**3.9**	**2.20**	**2.70**	4.70	**0.70**	38	16.72	21

Notes. VERITAS and Whipple fluxes were measured around seven hours after the MAGIC observations.

Table 3: Integral flux above 200 GeV and parameters of the two-zone SSC model. Bold-faced text is used to depict the model parameters that were varied to describe the SED during the 13-day period.

Date [MJD]	MAGIC flux [10^{-10}cm^{-2}s^{-1}]	VERITAS flux [10^{-10}cm^{-2}s^{-1}]	Whipple flux [10^{-10}cm^{-2}s^{-1}]	$\gamma_{\rm min}$ [10^4]	$\gamma_{\rm max}$ [10^5]	$\gamma_{\rm br1}$ [10^5]	$\gamma_{\rm br2}$ [10^5]	s_1	s_2	s_3	$n_{\rm e}$ [10^3cm^{-3}]	B [mG]	log(R) [cm]	δ
the quiescent blob														
Parameters fixed for all dates to those from MJD 55274 one-zone SSC				0.08	1000	0.35	3.9	2.2	2.7	4.7	0.9	38	16.72	21
the flaring blob														
55265	3.8 ± 0.2	4.0 ± 0.5		**3.0**	6	**3.0**	- -	2.0	3.0	- -	**5.0**	**105**	15.51	35
55266	4.7 ± 0.2			**3.0**	6	**3.0**	- -	2.0	3.0	- -	**6.0**	**100**	15.51	35
55267		4.0 ± 0.5	5.3 ± 0.3	**2.5**	6	**1.1**	- -	2.0	3.0	- -	**5.9**	**100**	15.51	35
55268	2.1 ± 0.3	4.0 ± 0.6	4.8 ± 0.3	**5.3**	6	**1.8**	- -	2.0	3.0	- -	**5.6**	**100**	15.51	35
55269	3.3 ± 0.3	4.2 ± 0.6	4.2 ± 0.3	**3.0**	6	**2.3**	- -	2.0	3.0	- -	**5.2**	**90**	15.51	35
55270	2.3 ± 0.2	2.6 ± 0.4	3.0 ± 0.2	**3.5**	6	**0.8**	- -	2.0	3.0	- -	**6.0**	**75**	15.51	35
55271		3.5 ± 0.4	4.1 ± 0.5	**3.5**	6	**1.2**	- -	2.0	3.0	- -	**6.5**	**75**	15.51	35
55272		2.5 ± 0.4		**3.5**	6	**2.0**	- -	2.0	3.0	- -	**3.0**	**75**	15.51	35
55273	1.5 ± 0.2	2.0 ± 0.4	2.5 ± 0.3	**3.5**	6	**0.5**	- -	2.0	3.0	- -	**4.0**	**75**	15.51	35
55274	1.0 ± 0.3	1.6 ± 0.3	1.9 ± 0.2	- -	- -	- -	- -	- -	- -	- -	- -	- -	- -	- -
55275			1.8 ± 0.3	**3.5**	6	**0.5**	- -	2.0	3.0	- -	**5.0**	**60**	15.51	35
55276	1.6 ± 0.2		1.5 ± 0.3	**3.5**	6	**1.0**	- -	2.0	3.0	- -	**3.0**	**60**	15.51	35
55277	1.2 ± 0.1		1.4 ± 0.4	**3.5**	6	**0.8**	- -	2.0	3.0	- -	**2.5**	**60**	15.51	35

Notes. On MJD 55274, Mrk 421 had the lowest broadband activity among all the 13 dates. The quiescent blob emission was fixed to the SED of this date, and consequently the emission of the flaring blob on this date is null.

Table 4: Peak positions and widths of the synchrotron and inverse-Compton bumps derived from the two-zone SSC model parameters reported in Table 3.

Date	$\nu^{\rm syn}_{\rm peak}$	$(\nu F_\nu)^{\rm syn}_{\rm peak}$	$\nu^{\rm syn}_1$	$\nu^{\rm syn}_2$	$\log(\nu^{\rm syn}_2/\nu^{\rm syn}_1)$	$\nu^{\rm ic}_{\rm peak}$	$(\nu F_\nu)^{\rm ic}_{\rm peak}$	$\nu^{\rm ic}_1$	$\nu^{\rm ic}_2$	$\log(\nu^{\rm ic}_2/\nu^{\rm ic}_1)$
- -	$[10^{17}]$	$[10^{-10}]$	$[10^{15}]$	$[10^{18}]$	- -	$[10^{25}]$	$[10^{-11}]$	$[10^{23}]$	$[10^{26}]$	- -
[MJD]	[Hz]	[erg cm^{-2}s^{-1}]	[Hz]	[Hz]	- -	[Hz]	[erg cm^{-2}s^{-1}]	[Hz]	[Hz]	- -
55265	8.1	7.9	34.	6.1	2.3	10.	15.	60.	9.5	2.2
55266	8.1	8.0	34.	5.9	2.2	10.	18.	94.	9.9	2.0
55267	4.0	5.5	11.	3.3	2.5	10.	17.	56.	5.1	2.0
55268	4.0	6.6	30.	4.5	2.2	17.	11.	16.	7.3	2.7
55269	4.0	6.1	1.9	4.5	2.4	10.	14.	42.	7.8	2.3
55270	2.0	3.9	5.7	2.3	2.6	6.0	10.	11.	4.3	2.6
55271	2.0	4.6	9.0	2.6	2.5	1.0	13.	30.	5.4	2.3
55272	4.0	3.8	4.9	2.8	2.8	3.4	11.	7.4	4.5	2.8
55273	2.0	3.1	3.1	1.9	2.8	1.9	7.7	3.9	3.0	2.9
55274	2.0	2.5	1.8	1.6	2.9	1.9	7.1	3.0	2.4	2.9
55275	2.0	3.0	2.8	1.8	2.8	3.4	7.9	4.2	3.0	2.9
55276	2.0	3.1	3.1	1.8	2.8	1.9	7.5	3.6	3.2	2.9
55277	2.0	2.9	2.7	1.7	2.8	1.9	7.4	3.4	2.8	2.9

Notes. $\nu^{\rm syn}_{\rm peak}$: the peak frequency of the synchrotron bump; $(\nu F_\nu)^{\rm syn}_{\rm peak}$: the peak energy flux of the synchrotron bump; $\nu^{\rm ic}_{\rm peak}$: the peak frequency of the inverse-Compton bump; $(\nu F_\nu)^{\rm ic}_{\rm peak}$: the peak energy flux of the inverse-Compton bump. For each bump in the SED, the value of $(\nu F_\nu)_{\rm peak}/2$ determines the two frequencies (ν_1 and ν_2) that are used to quantify the width of the bump in the logarithmic scale $\log(\nu_2/\nu_1)$.

Table 5: Jet powers and luminosities derived with the parameters from the one-zone SSC model reported in Table 2.

Date	N_e	$\langle\gamma_e\rangle$	L_e	L_p	L_B	U'_e/U'_B	L_{jet}	L_{syn}	L_{IC}	L_{ph}
- - -	$[10^{-1}]$	$[10^3]$	$[10^{43}]$	$[10^{43}]$	$[10^{42}]$	$[10^1]$	$[10^{44}]$	$[10^{42}]$	$[10^{41}]$	$[10^{42}]$
[MJD]	[cm^{-3}]	- - -	[erg s^{-1}]	[erg s^{-1}]	[erg s^{-1}]	- - -	[erg s^{-1}]	[erg s^{-1}]	[erg s^{-1}]	[erg s^{-1}]
55265	2.5	3.4	7.8	4.2	6.5	1.2	1.3	6.6	14.	8.1
55266	2.5	3.4	8.0	4.3	6.5	1.2	1.3	7.2	16.	8.8
55267	2.4	3.3	7.3	4.0	6.5	1.1	1.2	4.6	11.	5.7
55268	2.5	3.5	7.9	4.2	6.5	1.2	1.3	5.4	14.	6.7
55269	2.6	3.4	8.2	4.4	6.5	1.3	1.3	5.5	14.	6.9
55270	2.5	3.3	7.5	4.1	6.5	1.2	1.2	3.5	9.8	4.5
55271	2.5	3.4	7.6	4.1	6.5	1.2	1.2	4.0	11.	5.1
55272	2.5	3.3	7.5	4.1	6.5	1.1	1.2	3.7	10.	4.7
55273	2.5	3.2	7.3	4.1	6.5	1.1	1.2	3.1	8.7	4.0
55274	2.5	3.1	7.0	4.1	6.5	1.1	1.2	2.5	6.5	3.1
55275	2.3	3.2	6.8	3.9	6.5	1.1	1.1	2.8	7.2	3.5
55276	2.5	3.2	7.3	4.1	6.5	1.1	1.2	3.0	8.2	3.8
55277	1.9	3.3	5.8	3.2	6.5	.90	.97	2.6	5.7	3.2

Notes. N_e: total electron number density; $\langle\gamma_e\rangle$: mean electron Lorentz factor; L_e: jet power carried by electrons; L_p:the jet power carried by protons; L_B: jet power carried by the magnetic field; U'_e/U'_B: the ratio of comoving electron and magnetic-field energy densities; L_{jet}: total jet power; L_{syn}: the synchrotron luminosity; L_{IC}: inverse-Compton luminosity; L_{ph}: total photon luminosity from the SSC model. See the calculation explanation in Section 5.

Table 6: Jet powers and luminosities derived with the parameters from the two-zone SSC model reported in Table 3.

Date	N_e	$\langle\gamma_e\rangle$	L_e	L_p	L_B	U'_e/U'_B	L_{jet}	L_{syn}	L_{IC}	L_{ph}	$^{sum}L_e$	$^{sum}L_p$	$^{sum}L_B$	$^{sum}L_{jet}$	$^{sum}L_{syn}$	$^{sum}L_{IC}$	$^{sum}L_{ph}$
- - -	$[10^{-1}]$	$[10^4]$	$[10^{43}]$	$[10^{41}]$	$[10^{41}]$	$[10^1]$	$[10^{43}]$	$[10^{41}]$	$[10^{40}]$	$[10^{41}]$	$[10^{43}]$	$[10^{43}]$	$[10^{42}]$	$[10^{44}]$	$[10^{42}]$	$[10^{41}]$	$[10^{42}]$
[MJD]	[cm^{-3}]	- - -	[erg s^{-1}]	[erg s^{-1}]	[erg s^{-1}]	- - -	[erg s^{-1}]	[erg s^{-1}]	[erg s^{-1}]	[erg s^{-1}]	[erg s^{-1}]	[erg s^{-1}]	[erg s^{-1}]	[erg s^{-1}]	[erg s^{-1}]	[erg s^{-1}]	[erg s^{-1}]
the quiescent blob																	
- -	2.5	.31	7.0	410	65.	1.1	12.	25.	65.	31.							
the flaring blob											the quiescent blob + the flaring blob						
55265	1.6	9.0	1.4	2.8	5.3	2.6	1.5	13.	18.	15.	8.4	4.1	7.0	1.3	3.8	8.3	4.6
55266	1.9	9.0	1.7	3.4	4.8	3.4	1.7	13.	23.	15.	8.7	4.1	7.0	1.4	3.8	8.8	4.6
55267	2.1	6.5	1.3	3.8	4.8	2.8	1.4	7.9	18.	9.7	8.3	4.1	7.0	1.3	3.3	8.3	4.1
55268	.89	12.	1.1	1.6	4.8	2.2	1.1	9.5	8.8	10.	8.1	4.1	7.0	1.3	3.4	7.4	4.1
55269	1.6	8.6	1.4	2.9	3.9	3.5	1.4	8.7	15.	10.	8.4	4.1	6.9	1.3	3.4	8.0	4.1
55270	1.3	7.6	1.0	2.4	2.7	3.7	1.1	3.4	7.3	4.2	8.0	4.1	6.8	1.3	2.8	7.2	3.5
55271	1.6	8.4	1.3	2.9	2.7	4.8	1.4	5.0	12.	6.2	8.3	4.1	6.8	1.3	3.0	7.7	3.7
55272	.77	9.3	.71	1.4	2.7	2.6	.76	3.5	9.9	4.5	7.7	4.1	6.8	1.3	2.8	7.5	3.5
55273	.74	6.9	.50	1.3	2.7	1.9	.54	1.5	1.9	1.7	7.5	4.1	6.8	1.3	2.7	6.7	3.3
55274	- -	- -	- -	- -	- -	- -	- -	- -	- -	- -	7.0	4.1	6.5	1.2	2.5	6.5	3.1
55275	.93	6.9	.63	1.7	1.7	3.6	.66	1.2	2.2	1.5	7.6	4.1	6.7	1.3	2.6	6.7	3.2
55276	.70	8.0	.56	1.3	1.7	3.2	.59	1.3	1.7	1.5	7.6	4.1	6.7	1.3	2.6	6.7	3.2
55277	.56	7.6	.42	1.0	1.7	2.4	.45	.92	.95	1.0	7.4	4.1	6.7	1.2	2.6	6.6	3.2

Notes. N_e: total electron number density; $\langle\gamma_e\rangle$: mean electron Lorentz factor; L_e: jet power carried by electrons; L_p: jet power carried by protons; L_B: jet power carried by the magnetic field; U'_e/U'_B: ratio of comoving electron and magnetic-field energy densities; L_{jet}: total jet power; L_{syn}: synchrotron luminosity; L_{IC}: inverse-Compton luminosity; L_{ph}: total photon luminosity from the SSC model. See the calculation explanation in Section 5. The quantities with the ^{sum} superscript report the sums of the quantities from the quiescent and the flaring blob.

3.1 – Variability Mrk501

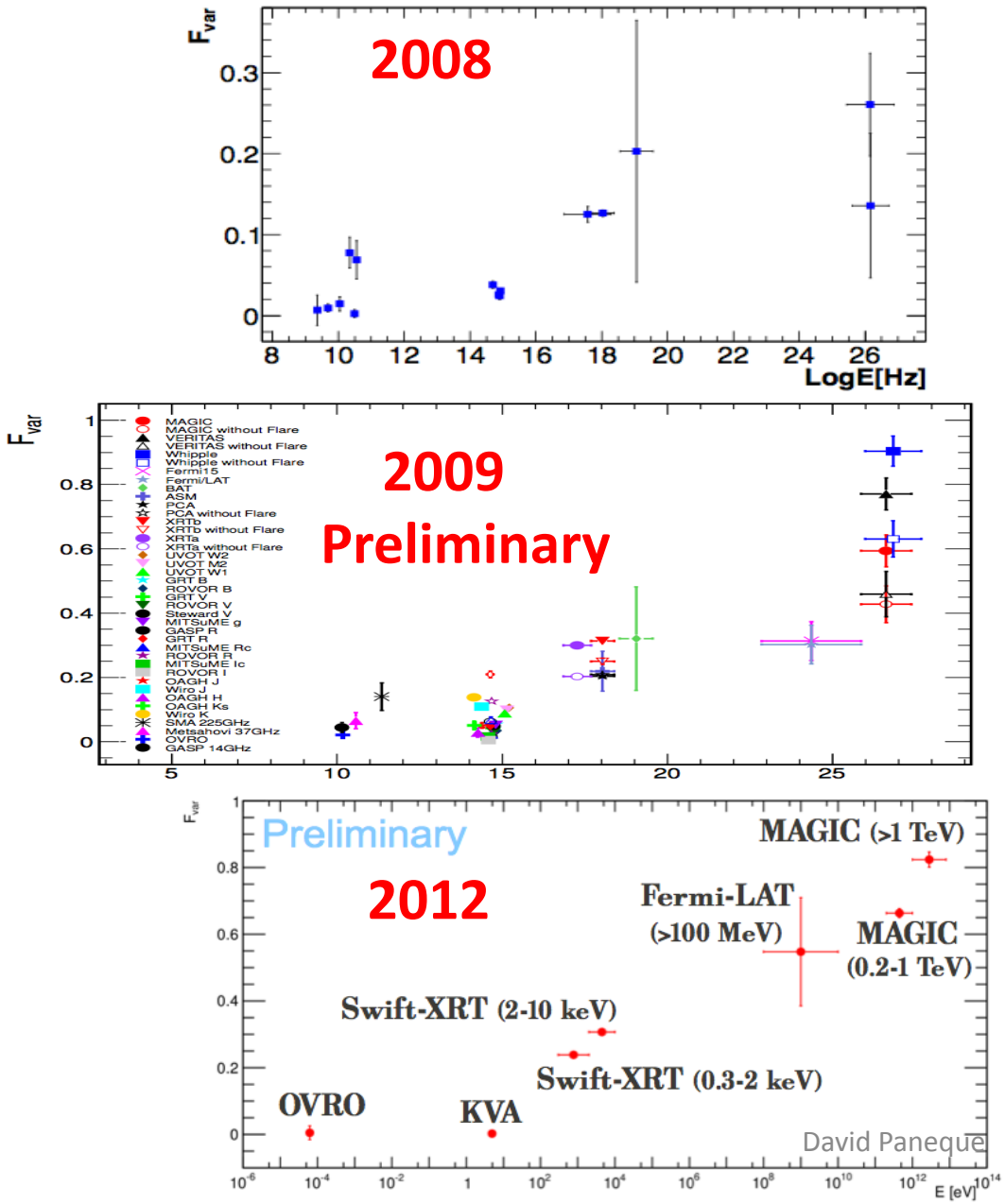

Similar pattern to the one observed for Mrk421

Highest variability at X-rays and VHE.

Although for Mrk501, the variability at VHE is relatively higher than that measured for X-rays (with respect to what is observed for Mrk421)

3.1 – Variability Mrk501

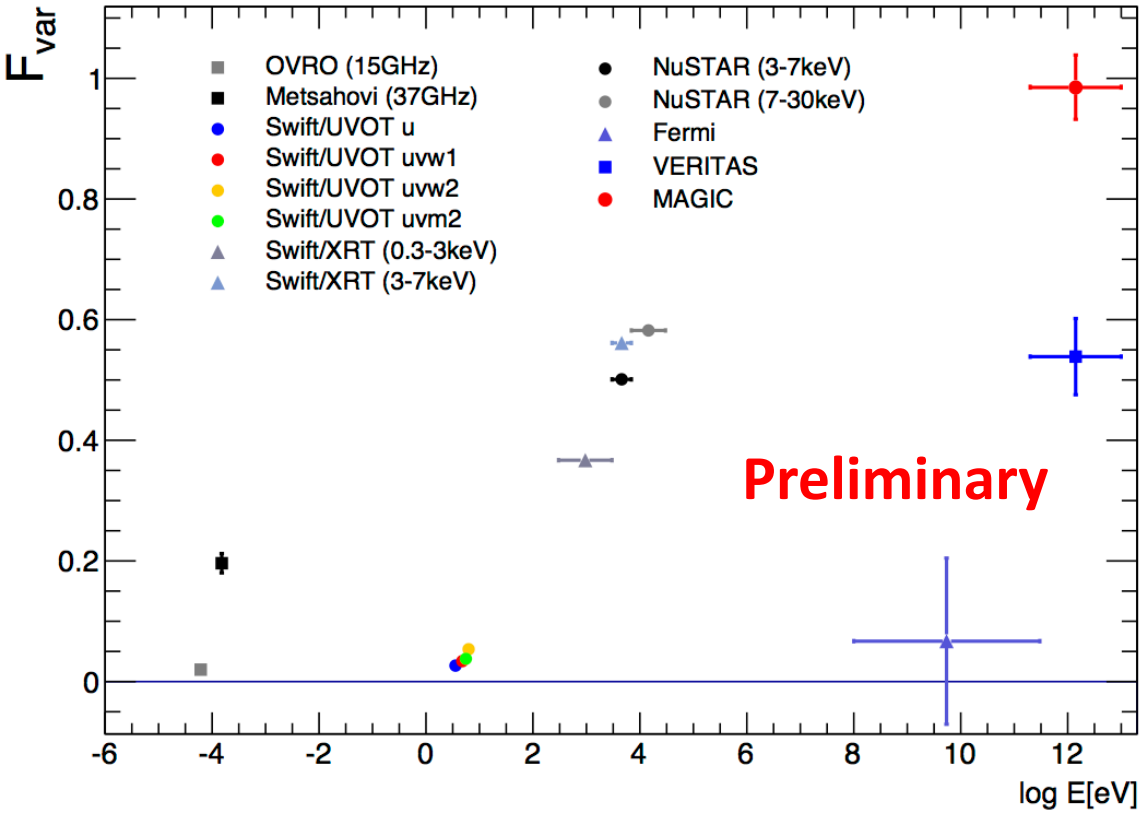

Mrk501 2013

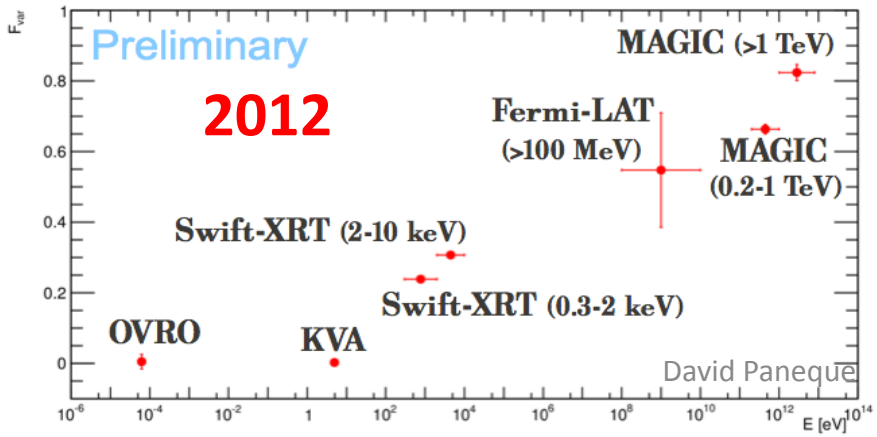

See poster presentation from Amy Furniss (8.11)

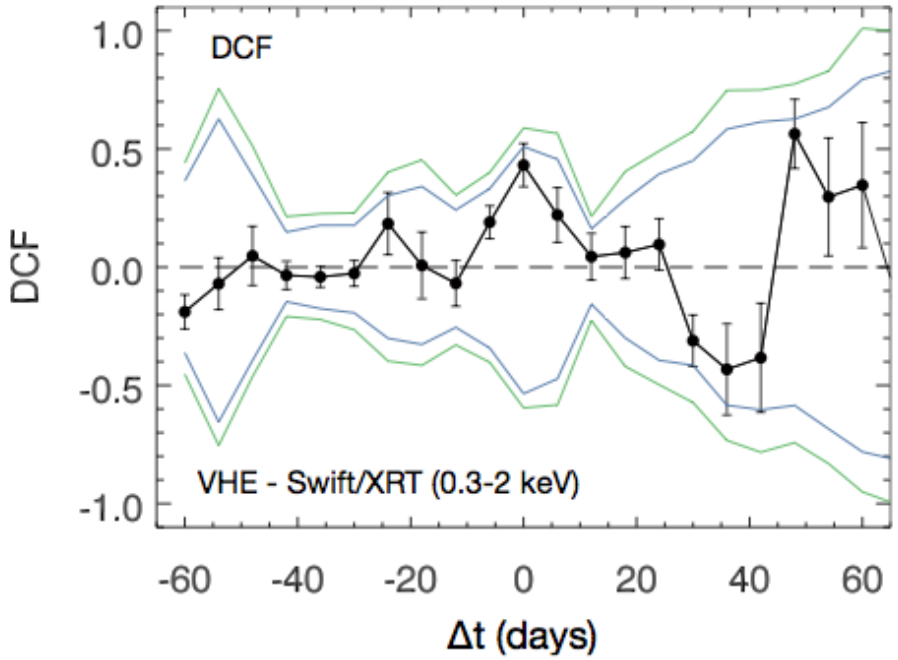

Fig. 6. DCF of the combined Whipple and MAGIC ("VHE") light curve, correlated with the *Swift*/XRT (0.3-2 keV) light curve. The black error bars represent the uncertainties as derived from Edelson & Krolik (1988). The green lines represent the 1% and 99% extremes of the DCF distribution of simulated *Swift*/XRT light curves when correlated with the measured VHE light curve. The blue lines represent the 5% and 95% extremes.

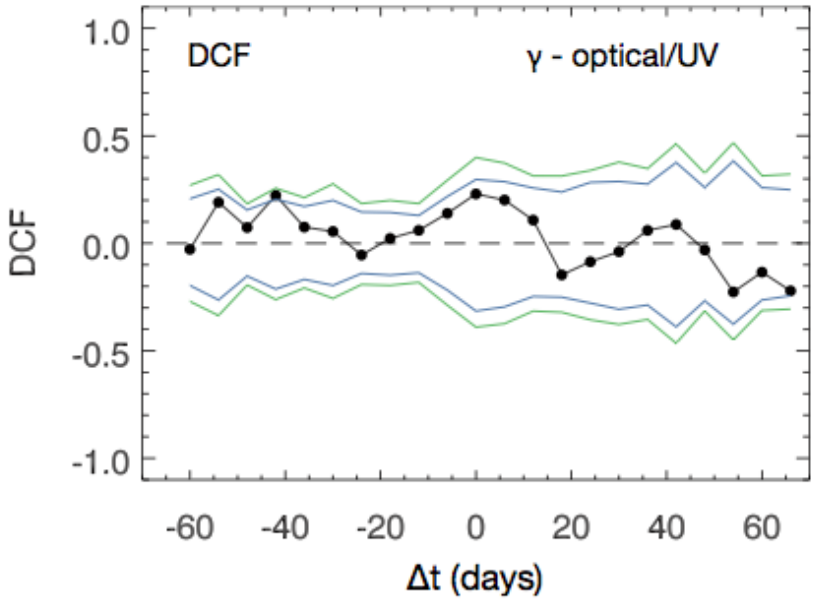

Fig. 7. The average DCF of the *Fermi*-LAT HE γ-ray light curve, correlated with the optical and UV light curves (GASP *R*-band, GRT *BVRI*, MITSuME g, MITSuME Ic and UVOT W1), is shown in black. The green lines represent the 1% and 99% extremes of the likewise averaged DCF distribution of simulated optical/UV light curves when correlated with the real *Fermi*-LAT light curve. The blue lines represent the 5% and 95% extremes.

3.2 – Correlations

Mrk501

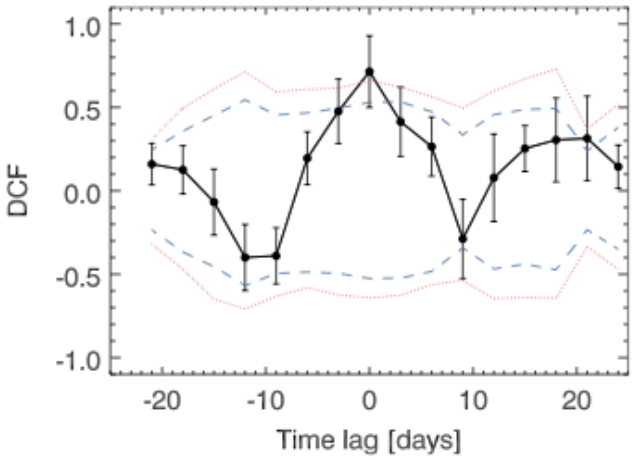

(a) *RXTE*/PCA vs. *Swift*/XRT

Little variability in 2008
(see marginal correlation
RXTE with SwiftXRT)

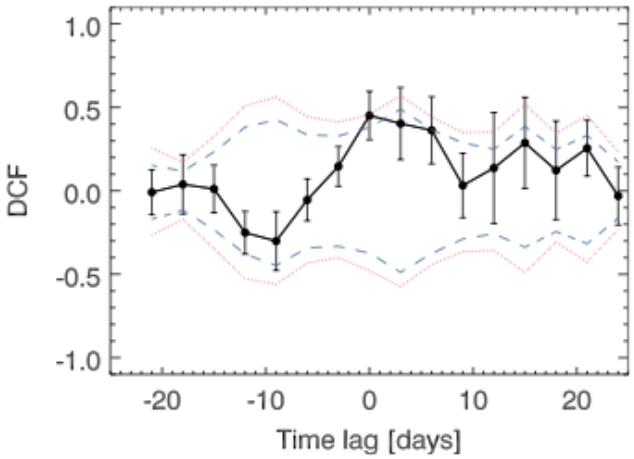

(b) *RXTE*/PCA vs. MAGIC & VERITAS

Marginal correlation
for X-ray and VHE

3.2 – Correlations

X-ray and VHE light curves (Mrk501@MW2008)

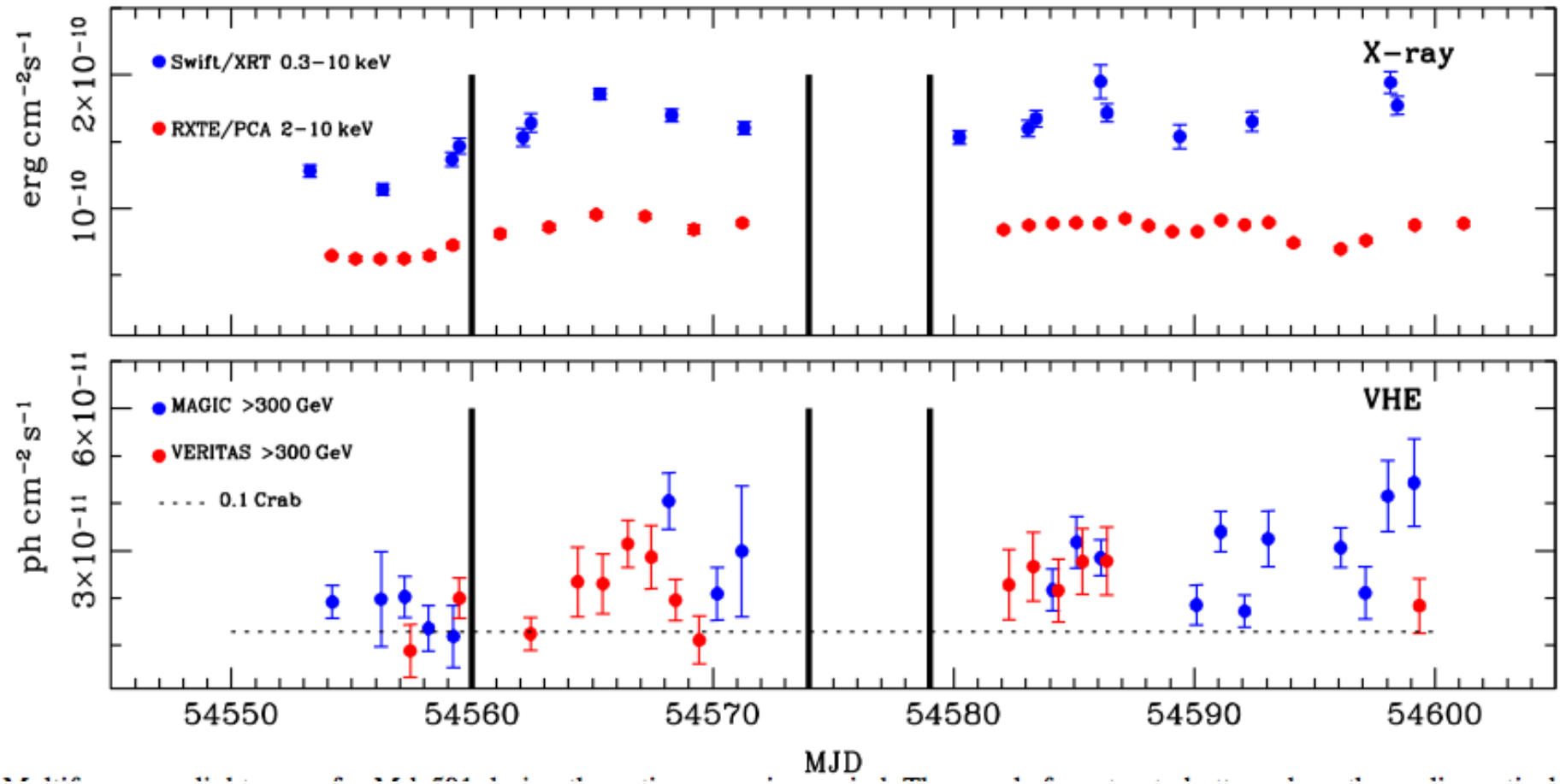

Very low activity + very low variability

Mrk501 2009

Zoom to Light curve during May 2009

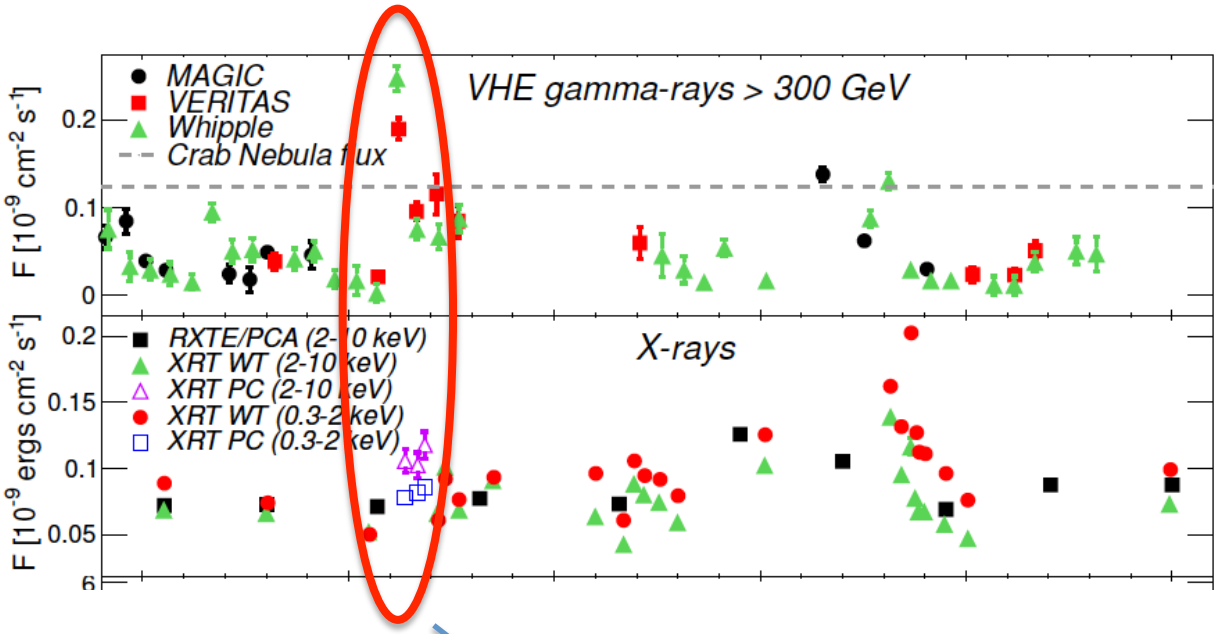

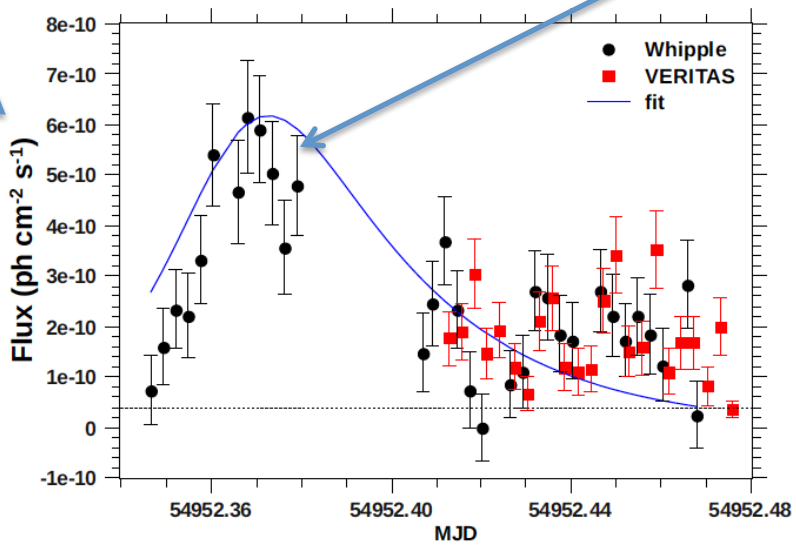

Peak shows ~4 Crabs, which were reached in ~25 min

From the light curve, it seems that there is no much activity in X-rays
Orphan flare ???
Never observed for Mrk501

When looking into X-ray spectral index, one can see that the TeV flare comes at the same time as a hardening in the spectra, which does NOT occur for the second TeV flare (3 weeks after the first TeV flare)

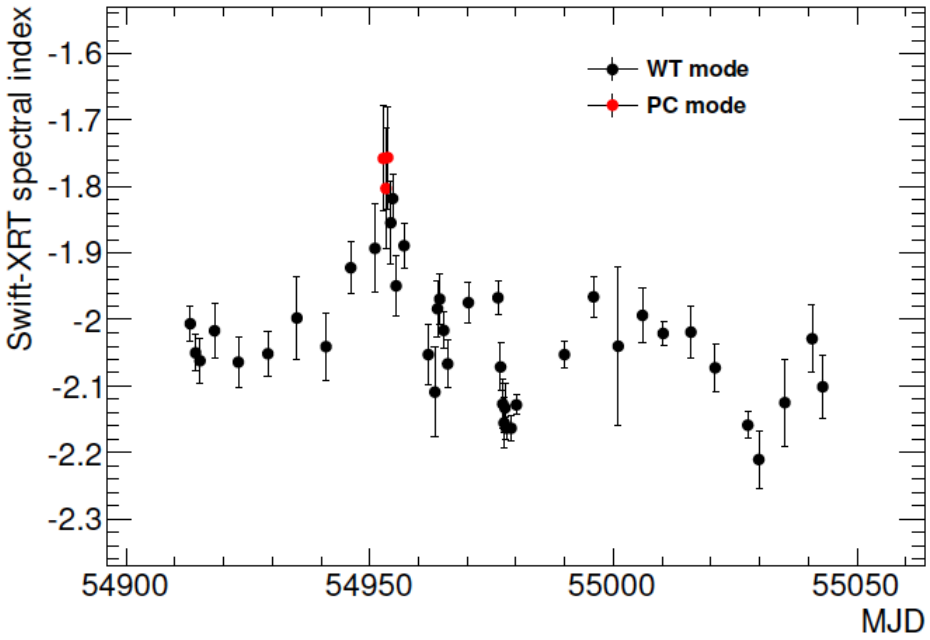

Figure 7: Spectral index obtained from simple power-law fit to *Swift*-XRT spectra vs. time. A significant hardening of the spectrum around MJD 54955 can be noted.

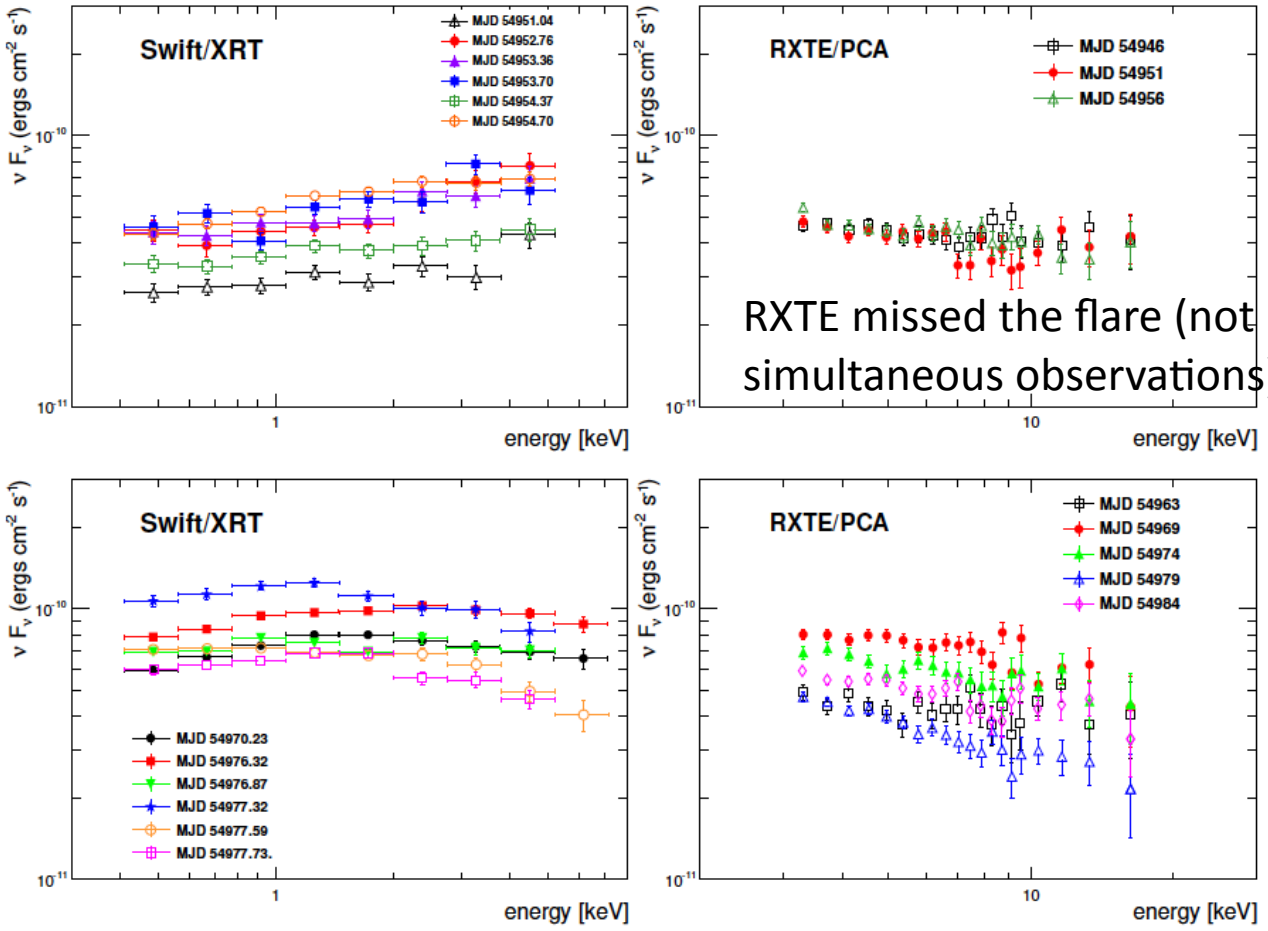

First flare

Second flare

Figure 6: X-ray spectra from single pointings of the instruments. Left hand side: *Swift*-XRT. Right hand side: *RXTE*-PCA. Upper panel: Around first flare; lower panel: spectra around second flare.

Mrk501 2009

Fractional variability vs energy band

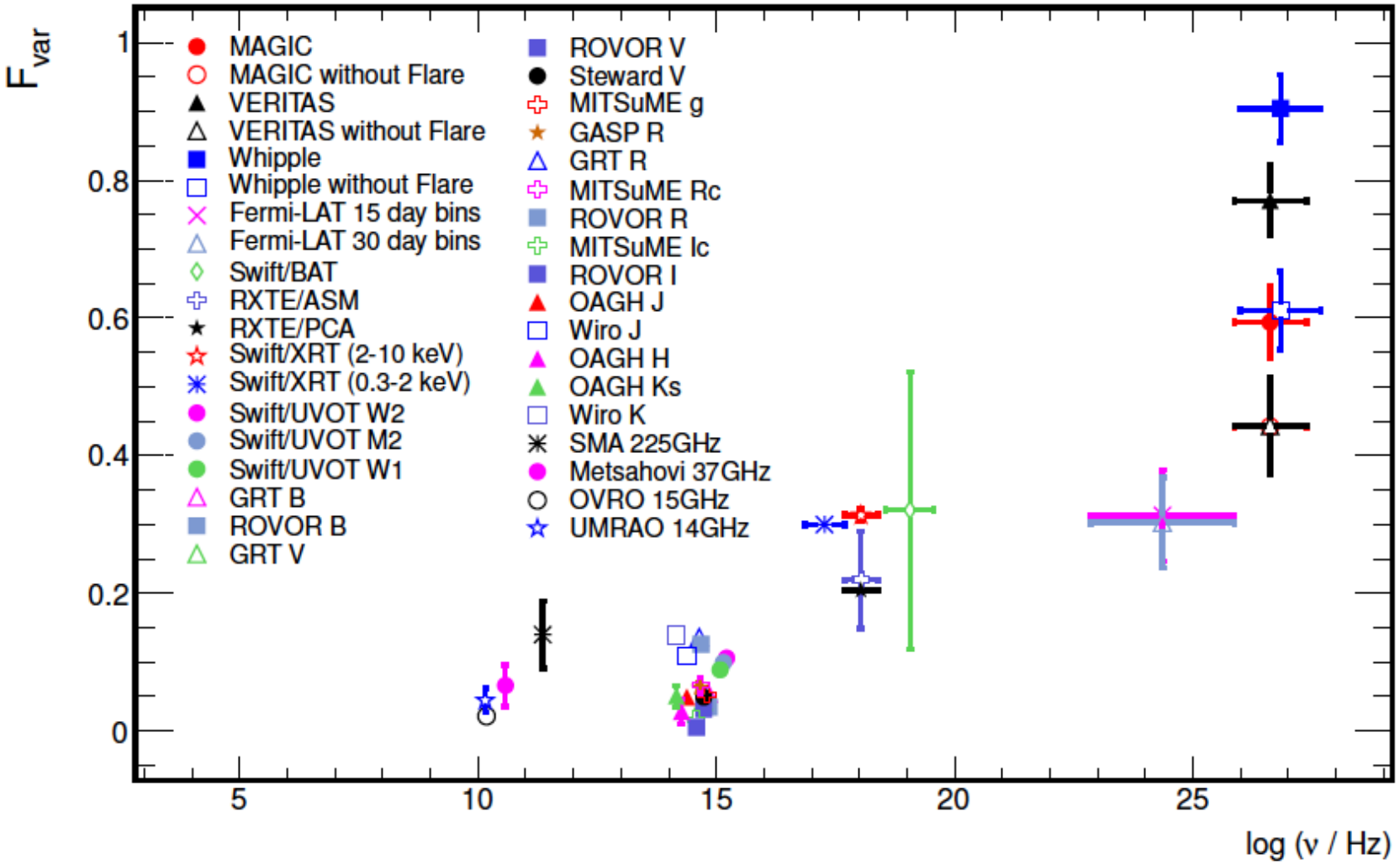

The band with highest variability is VHE (not X-rays, as for Mrk421)

Good agreement in Fvar among VHE after subtracting the flares

Similar to situation reported for BL Lac (LBL) in the Nature paper from Marscher 2008

Polarization change – the case of BL Lacertae (LBL)

Marscher, A. P. et al. (2008) *Nature, 452* (7190), 966–969.

VHE emission seen by MAGIC

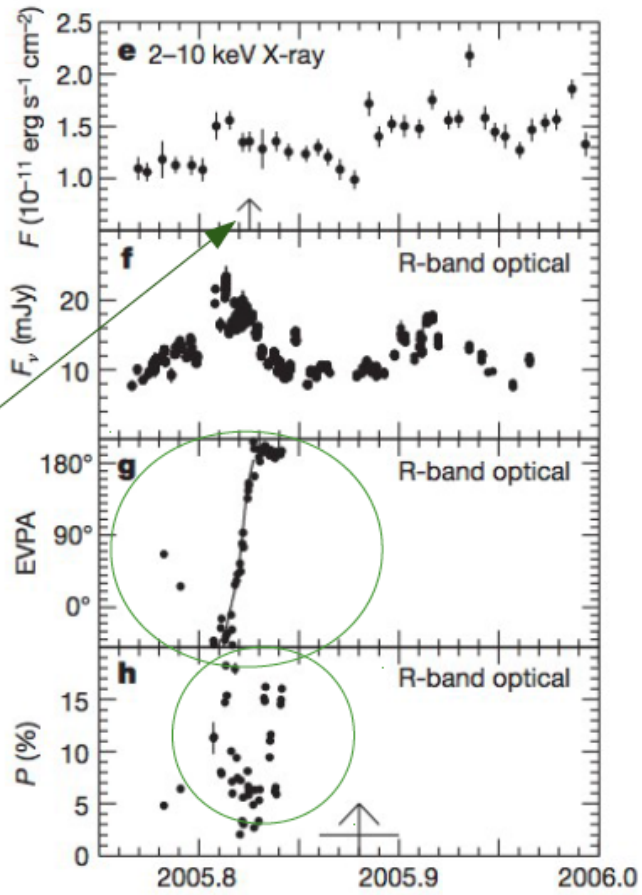

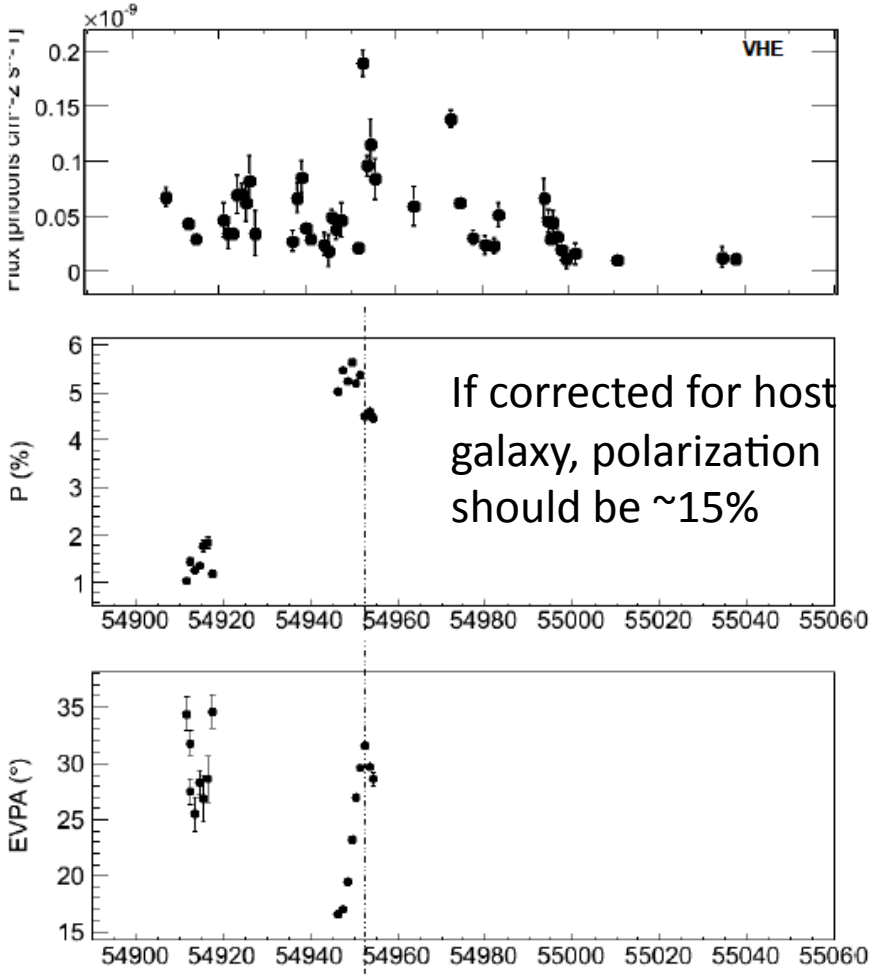

If corrected for host galaxy, polarization should be ~15%

Possible scenario (proposed by Marscher)

Polarization change – the case of BL Lacertae

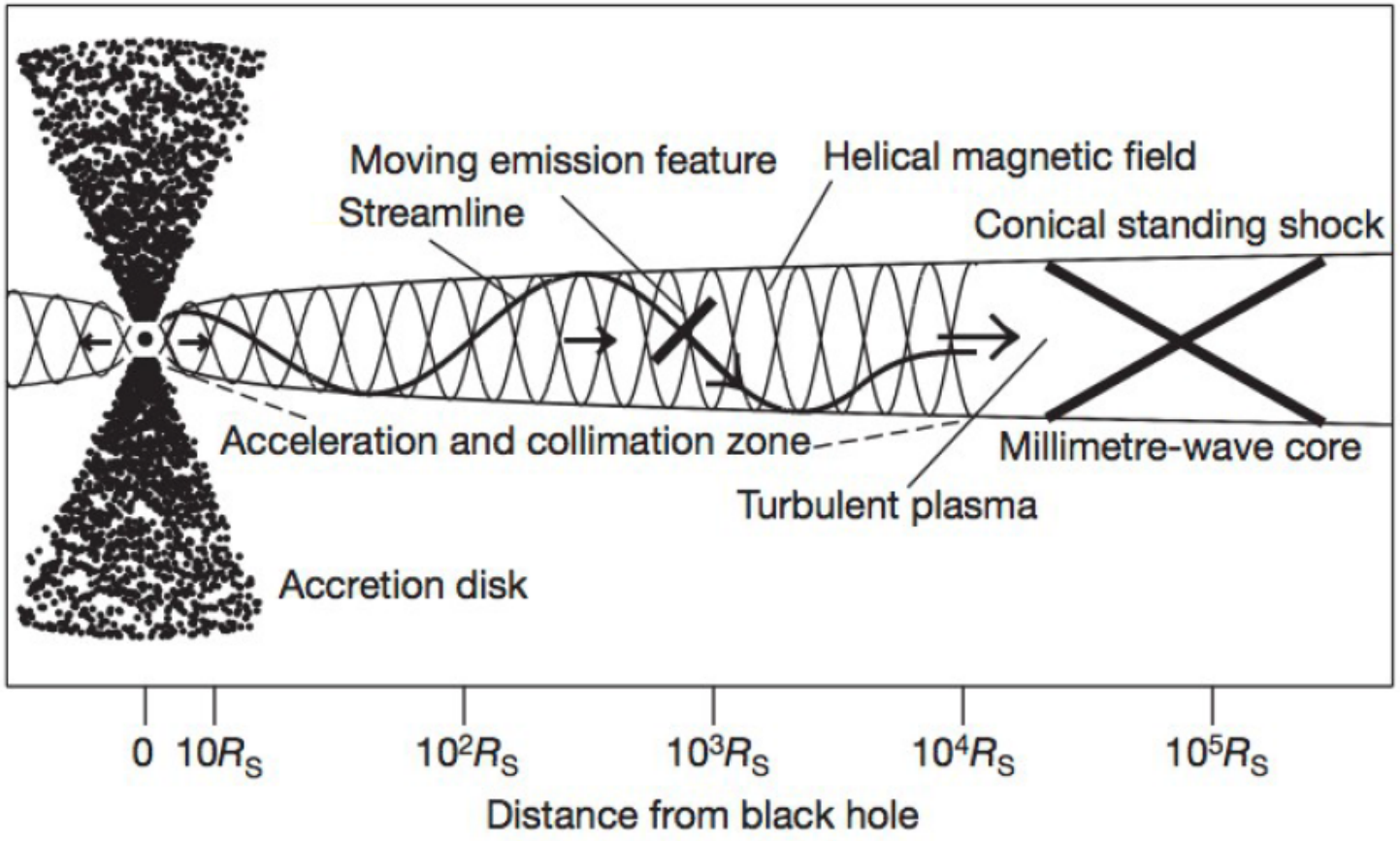

Marscher, A. P. et al. (2008) *Nature*, *452*(7190), 966–969.

FSRQ PKS1510-089

Marscher et al, 2010, ApJL, 710

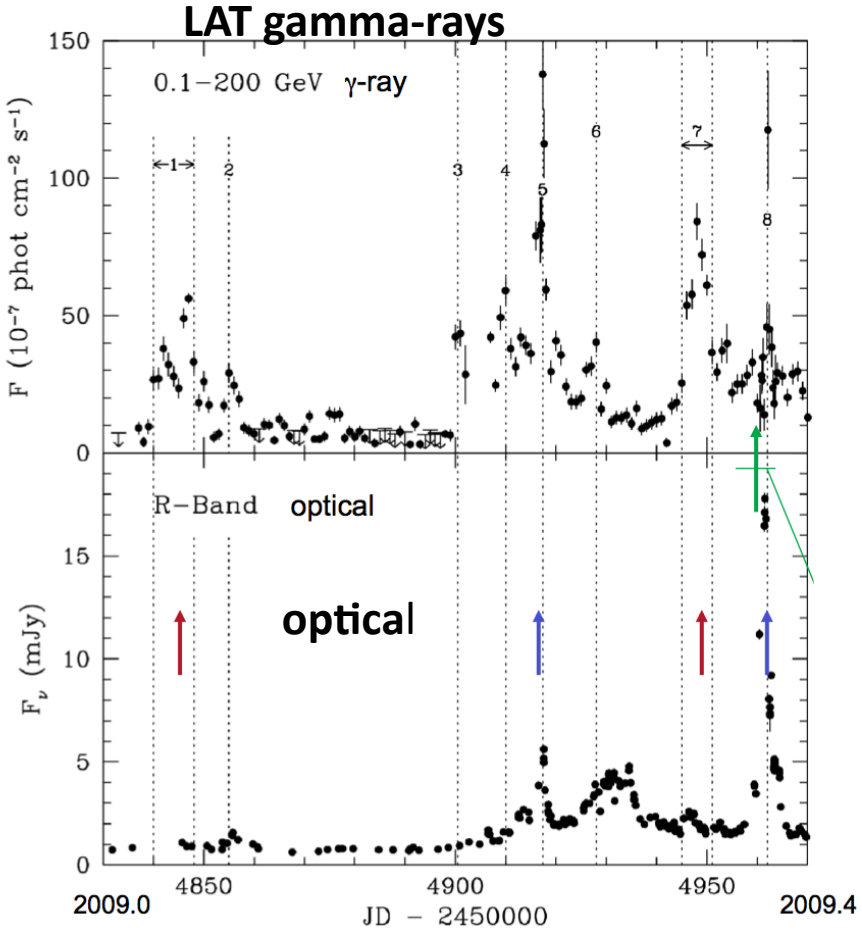

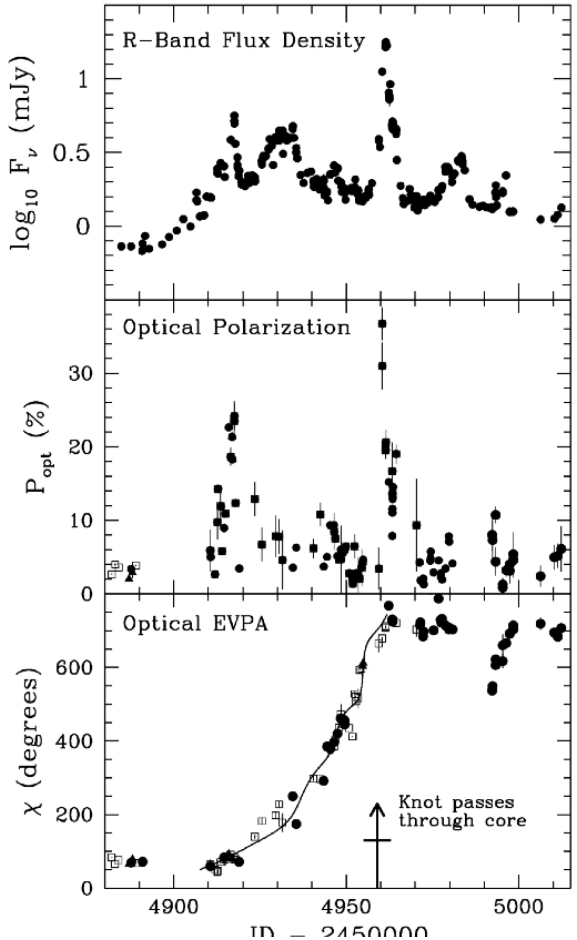

Optical flux (R band)

Optical polarization

polarization angle

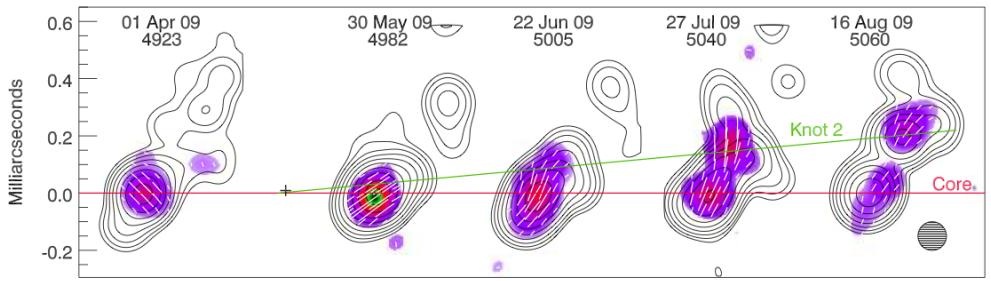

VLBA 43 GHz

Sites of γ-ray Flares in PKS 1510-089 (Marscher et al. 2010 ApJL)